Multi-zone modelling of partially premixed low-temperature combustion in pilot-ignited natural-gas engines

S R Krishnan and K K Srinivasan

Proceedings of the Institution of Mechanical Engineers, Part D: Journal of Automobile Engineering 2010 224: 1597
DOI: 10.1243/09544070JAUTO1472

Multi-zone modelling of partially premixed low-temperature combustion in pilot-ignited natural-gas engines

S R Krishnan* and **K K Srinivasan**
Department of Mechanical Engineering, Mississippi State University, Starkville, Mississippi, USA

The manuscript was received on 25 December 2009 and was accepted after revision for publication on 29 June 2010.

DOI: 10.1243/09544070JAUTO1472

Abstract: Detailed results from a multi-zone phenomenological simulation of partially premixed advanced-injection low-pilot-ignited natural-gas low-temperature combustion are presented with a focus on early injection timings (the beginning of (pilot) injection (BOI)) and very small diesel quantities (2–3 per cent of total fuel energy). Combining several aspects of diesel and spark ignition engine combustion models, the closed-cycle simulation accounted for diesel autoignition, diesel spray combustion, and natural-gas combustion by premixed turbulent flame propagation. The cylinder contents were divided into an unburned zone, several pilot fuel zones (or 'packets') that modelled diesel evaporation and ignition, a flame zone for natural-gas combustion, and a burned zone. The simulation predicted the onset of ignition, cylinder pressures, and heat release rate profiles satisfactorily over a wide range of BOIs (20–60° before top dead centre (before TDC)) but especially well at early BOIs. Strong coupling was observed between pilot spray combustion in the packets and premixed turbulent combustion in the flame zone and, therefore, the number of ignition centres (packets) profoundly affected flame combustion. The highest local peak temperatures (greater than 2000 K) were observed in the packets, while the flame zone was much cooler (about 1650 K), indicating that pilot diesel spray combustion is probably the dominant source of engine-out emissions of nitrogen oxide (NO_x). Further, the 60° before TDC BOI yielded the lowest average peak packet temperatures (about 1720 K) compared with the 20° before TDC BOI (about 2480 K) and 40° before TDC BOI (about 2700 K). These trends support experimental NO_x trends, which showed the lowest NO_x emissions for the 60°, 20°, and 40° before TDC BOIs in that order. Parametric studies showed that increasing the intake charge temperature, pilot quantity, and natural-gas equivalence ratio all led to higher peak heat release rates and hotter packets but the pilot quantity and intake temperature affected the potential for NO_x formation to a greater extent.

Keywords: phenomenological model, low-temperature combustion, dual-fuel engines, pilot ignition, micropilot, natural gas, Shell ignition model

1 INTRODUCTION

The continuing drive to adopt clean alternative fuels and to reduce dependence on conventional petroleum fuels has stimulated the substitution of natural gas (among other fuels) for gasoline and diesel in internal combustion engines. Despite fluctuating natural-gas prices, natural-gas-fuelled engines remain commercially viable for several applications: transportation, distributed electric power generation, gas production, gas pipeline compression, and petroleum-refining operations. However, the challenge with employing natural gas as an engine fuel stems from the fact that it is primarily composed of methane, which is very difficult to ignite. Several ignition strategies including lean-burn spark ignition [**1**], laser ignition [**2**, **3**], and pilot ignition [**4**–**8**] have been utilized to increase efficiencies and to decrease emissions from natural-gas engines. Of these, pilot

**Corresponding author: Department of Mechanical Engineering, Mississippi State University, PO Box 9552, Mississippi State, MS 39762, USA.*
email: krishnan@me.msstate.edu

ignition, which uses small diesel sprays as the ignition sources, offers the advantages of multiple ignition centres and higher energy densities compared with conventional spark ignition. Gebert *et al.* [**9**] showed that the energy associated with a pilot diesel spray volume of 1 mm^3 is approximately two orders of magnitude greater than the energy provided by a spark. Therefore, the quality of ignition is better with diesel pilot ignition, and spatially dispersed, multiple-ignition centres lead to faster burn rates compared to single-point ignition sources.

In pilot-ignited natural-gas engines, the natural-gas–air mixture is inducted during the intake stroke and ignited towards the end of compression by small diesel sprays. These dual-fuel engines yield low oxides of nitrogen (NO_x) and particulate matter (PM) emissions and fuel conversion efficiencies comparable with conventional diesel engines. However, high unburned hydrocarbon (HC) emissions, cycle-to-cycle variations at low loads, and tendency to knock at high loads are known problems in dual-fuel engines [**6**]. One approach for retaining the NO_x benefits of dual-fuel engines is maximization of natural-gas substitution or minimization of diesel usage [**8**]. To reduce NO_x emissions further without compromising HC emissions or fuel conversion efficiency, more sophisticated diesel injection systems (than conventional mechanical injection systems) that can consistently and reliably meter very small diesel quantities are required [**7**]. Better pilot injection systems will also enable dual-fuel low-temperature combustion (LTC) strategies to be adopted.

For conventional spark ignition (SI) and compression ignition engine combustion, Flynn *et al.* [**10**] concluded that engine-out NO_x emissions are inevitable and may not be decreased below a limit because the local in-cylinder temperatures are usually higher than 2000 K. Therefore, to meet future emissions standards and to increase fuel conversion efficiencies simultaneously, LTC concepts that can provide controlled engine operation at high engine loads (brake mean effective pressure (BMEP), greater than 10 bar) are desirable. Different approaches have been investigated to realize LTC operation with gasoline and diesel fuels. These include, among others, homogeneous charge compression ignition (HCCI) [**11**], early-injection LTC (e.g. the UNIBUS concept [**12**]), late-injection LTC with aggressive exhaust gas recirculation (EGR) and swirl ratios [**13**], and partially premixed LTC [**14–16**] with low-cetane fuels. Combustion control issues with HCCI limit the maximum attainable BMEPs. To provide better control of the combustion process, other LTC concepts utilize early or late direct fuel injection. Although early- and late-injection LTC concepts have their own advantages and drawbacks, the key idea in both approaches is to ensure that the end of fuel injection (EOI) is separated from the start of combustion (SOC) by 'sufficiently long' ignition delay periods [**17**]. By comparison, both fuel injection and combustion events occur simultaneously in conventional diesel engines, resulting in high NO_x and PM emissions. Consequently, this separation between the EOI and the SOC is necessary to reap the NO_x and PM benefits of LTC.

Kalghatgi and co-workers [**14–16**] achieved controlled LTC at relatively high loads (indicated mean effective pressure (IMEP), approximately 15 bar) by resorting to partially premixed combustion with gasoline. They demonstrated that late injection of gasoline yielded low NO_x and PM emissions by increasing ignition delays substantially compared with diesel fuels. Since diesel is easier to autoignite than gasoline, the maximum allowable engine loads in diesel-fuelled LTC HCCI are lower than for gasoline. These results indicate that low-cetane fuels that are highly resistant to autoignition (e.g. gasoline and natural gas) can yield controlled LTC over a wide range of engine operating conditions.

2 ADVANCED-INJECTION LOW-PILOT-IGNITED NATURAL-GAS COMBUSTION

Dual–fuel experiments [**18–20**] performed with a common-rail low-pilot-injection system established that engine-out NO_x emissions can be reduced to about 0.2 g/kW h over a wide range of engine loads when very small diesel sprays (providing 2–3 per cent of total fuel energy) are injected early in the compression stroke (about 60° before top dead centre (before TDC)) to ignite premixed natural-gas–air mixtures. The penalty on fuel conversion efficiencies was minimal despite the remarkable reduction in NO_x emissions; however, HC and carbon monoxide (CO) emissions increased substantially at advanced injection timings. This partially premixed LTC concept has been termed advanced-injection low-pilot-ignited natural-gas (ALPING) combustion [**20**]. By combining a low-cetane main fuel (natural gas) and early injection of a high-cetane pilot fuel (diesel), the EOI and the SOC were separated to achieve controlled LTC for a BMEP of up to 12 bar.

It is hypothesized that the ALPING combustion process combines some aspects of both conventional diesel and SI engine combustion. Early in-

jection (the beginning of (pilot) injection (BOI)) of pilot diesel leads to a very long ignition delay period because the local in-cylinder temperatures at BOI are not conducive to ignition. Over the long ignition delay period, the pilot sprays disperse and mix with the surrounding natural-gas–air mixture. When the piston approaches top dead centre (TDC) and the local temperatures become high enough to initiate and sustain rapid pre-ignition reactions, the diesel autoignites (simultaneously or in rapid succession) at different locations inside the cylinder. These spatially distributed ignition centres foster the creation of several 'flamelets' that result in localized flame propagation through the lean mixture of natural gas (mostly methane) and air. These distributed flamelets ensure large enflamed areas, thus resulting in faster energy release rates and good fuel conversion efficiencies.

The range of equivalence ratio (ϕ) values (based on both diesel and natural gas) encountered in ALPING combustion lies between 0.2 (for low loads) and 0.6 (for high loads). Whereas it was previously thought that flame propagation in methane–air mixtures was limited to a lean flammability limit of $\phi \approx 0.5$ for atmospheric flames, *recent numerical simulations [**21**] suggested that, once ignition is achieved, flame propagation may occur even at much leaner equivalence ratios ($\phi \approx 0.2$) under engine-like conditions of temperature and pressure*. This evidence supports the hypothesis that flame propagation may occur from multiple ignition centres in ALPING combustion.

The research of Kalghatgi and co-workers [**14**–**16**] emphasizes the performance and emissions benefits of partially premixed LTC strategies. The ALPING combustion process is a partially premixed LTC concept realized with a specific combination of two fuels: an easily ignitable fuel (e.g. diesel) is used to initiate lean premixed combustion of a relatively difficult-to-ignite fuel (e.g. natural gas). Since diesel is just sufficiently (but not completely) premixed with the natural-gas–air mixture, ALPING combustion occurs at locally lean equivalence ratios for early BOIs, thereby leading to lower local temperatures and very low NO_x emissions. Further, with lean premixed ALPING combustion, PM emissions are also expected to be insignificant compared with conventional diesel combustion. High HC and CO emissions and poor low-load engine stability with ALPING combustion were addressed in hot EGR experiments [**22**, **23**], which yielded 70 per cent HC emissions reduction, efficiency improvement by 5 percentage points, and more stable engine operation with virtually no NO_x penalty at BMEPs of 6 bar and 3 bar. Also, the earliest possible BOI was extended from 60° before TDC without EGR to 70° before TDC with hot EGR.

3 OBJECTIVES

A phenomenological simulation that provides a framework for predicting dual-fuel, partially premixed LTC can be employed to gain deeper insights into ALPING combustion, especially at early BOIs, which yielded very low NO_x emissions. Phenomenological combustion models are routinely used to simulate performance and emissions in diesel engines [**24**–**26**]. For simulating dual-fuel engine combustion, several models have been developed. They range from relatively simple two-zone models [**27**] to increasingly complex multi-zone models [**28**] (some of which include detailed chemical kinetics [**29**–**31**]), and multi-dimensional models [**32**]. These models predict conventional dual-fuel engine performance and emissions satisfactorily. However, as discussed above, ALPING combustion differs significantly from conventional dual-fuel engine combustion. A review of the literature revealed that no existing models have been developed to simulate dual-fuel, partially premixed LTC explicitly at very early BOIs. Consequently, the specific objectives of the present work are as follows:

(a) to develop a multi-zone phenomenological simulation of ALPING combustion and to predict the cylinder pressure and heat release histories over a range of BOIs, with specific emphasis on understanding combustion at early BOIs (50–60° before TDC);
(b) to use the ALPING combustion simulation to investigate the effects of the intake manifold temperature, pilot fuel quantity, and natural-gas equivalence ratios for the early BOI of 60° before TDC.

4 MODEL DEVELOPMENT

A multi-zone phenomenological combustion model that simulates closed-cycle engine processes has been developed. The primary objective of the model is to simulate early-BOI ALPING combustion, which is significantly more difficult to predict than retarded-BOI combustion. In ALPING combustion, the initial pilot combustion phase is somewhat similar to diesel spray combustion while the subsequent natural-gas combustion phase involves premixed

turbulent combustion by flame propagation (similar to an SI engine). Therefore, the present model incorporates phenomenological aspects of both diesel spray combustion and premixed turbulent flame propagation.

The simulation starts from intake valve closure (IVC) and proceeds until exhaust valve opening. Depending on the stage of the simulation, the cylinder contents are divided into one or more of the following zones: an unburned zone, pilot fuel zones (packets), a flame zone, and a burned zone, as shown schematically in Fig. 1. While the different zones are illustrated as continuous and contiguous for ease of visualization, it should not be construed that they are necessarily so; in fact, at advanced BOIs, packets can be dispersed throughout the cylinder, forming distributed ignition centres. Since the simulation is only quasi-dimensional and is not capable of providing spatial resolution of the cylinder contents, it does not require any of these zones to be continuous or contiguous.

The generic form of the energy equation for a given zone i (an open thermodynamic system) is

$$\frac{\mathrm{d}(m_i c_{vi} T_i)}{\mathrm{d}\theta} = \sum_{\text{net in}} \frac{\mathrm{d}Q_i}{\mathrm{d}\theta} - \frac{P\,\mathrm{d}V_i}{\mathrm{d}\theta} + \sum_{\text{net in}} h_i \frac{\mathrm{d}m_i}{\mathrm{d}\theta} \qquad (1)$$

where m_i is the mass, c_{vi} is the specific heat at constant volume, T_i is the temperature, and all derivatives are with respect to the crank angle (CA) θ. The first term on the right-hand side of equation (1) is the net heat input into the zone, which includes heat transfer from and to the cylinder walls and, if applicable, energy lost owing to diesel evaporation and energy added owing to combustion in the packets or the flame zone. The second and third terms represent the boundary work output and the net enthalpy input due to any mass transfer respectively. Of these energy interactions, heat transfer and boundary work are experienced by all zones. Specific details of energy and mass interactions, together with the submodels used in different zones, are discussed later.

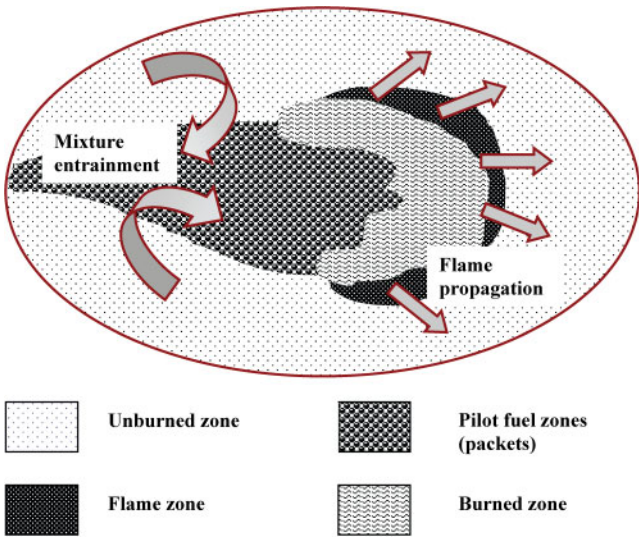

Fig. 1 Conceptual schematic diagram of zone evolution in the multi-zone simulation

4.1 Model assumptions

The important assumptions of the phenomenological ALPING combustion simulation are listed below.

1. Each zone is treated as an open thermodynamic system consisting of a mixture of ideal gases.
2. Heat transfer occurs only between each zone and the cylinder walls. Although mass transfer is allowed between zones, interzonal heat transfer is neglected.
3. Since the natural gas used in ALPING combustion experiments was largely composed of methane (98 vol %), methane is assumed to represent natural gas in the simulation and n-dodecane is assumed to represent diesel fuel.
4. When diesel and natural gas burn in any zone, they are converted into products of complete combustion (carbon dioxide (CO_2) and water (H_2O)).
5. The end of combustion (EOC) is attained when the unburned zone mass becomes very small (less than 0.001 per cent of its initial value) or more than 99.9 per cent of the total entrained mass in the flame zone has been burned.

4.2 Unburned zone

At IVC, the premixed natural-gas-air mixture trapped in the cylinder constitutes the unburned zone. Mass is transferred from the unburned zone to packets after the BOI and to the flame zone after the SOC. The state of the unburned zone is tracked as long as there is some unburned mass in the cylinder.

4.3 Pilot fuel zones (packets)

At the BOI, the packets, which account for combustion of diesel and some natural gas entrained in the diesel spray, come into existence. The lifetime of a packet depends on the fulfilment of certain 'dumping criteria' that are discussed later (see the descrip-

tion of the burned zone). A user-specified number of packets is sequentially injected throughout the injection duration and an axisymmetric diesel spray is assumed. As shown in Fig. 2, packets are classified on the basis of their time of entry into the cylinder (I) and the anticipated radial stratification in unburned mixture entrainment across the spray (J). In other words, J packets of equal diesel mass are injected every time step over the duration of injection, leading to a constant rate of fuel injection. A higher value of I indicates that the packet is injected relatively later in the injection process, while a higher value of J indicates that the packet's location is closer to the spray axis and less capable of entraining unburned mixture. Although spatial packet locations are not determined in this model, this method of packet identification allows appropriate stratification of mixture entrainment across the spray, and, in this sense, the entrainment model is quasi-dimensional. In the following paragraphs, various submodels relevant to the packets including mixture entrainment, diesel evaporation, ignition, and diesel and natural-gas combustion are discussed.

4.3.1 *Mixture entrainment model*

The phenomenological basis of the entrainment model is the recognition that the mixture entrainment into the spray is simultaneously governed by several factors. Since the spray can entrain unburned mixture only if it is available, the entrainment rate is proportional to the unburned-zone mass m_u. Further, all the available unburned mixture can be entrained into the spray in a characteristic entrainment time θ_{ch}, which is assumed to be the time taken (in degrees CA) for the spray to penetrate a characteristic entrainment distance equal to the cylinder bore radius. From a physical perspective, θ_{ch} can be interpreted as the time taken to entrain the surrounding fluid completely into the diesel spray or the time taken for the diesel spray to engulf the entire combustion chamber volume. To calculate θ_{ch}, spray penetration is determined using the correlation recommended by Dent [**33**]. While other more sophisticated spray penetration models (e.g. the Siebers [**34**] model) are certainly available, the Dent model has been adopted in the present work because it is more straightforward to implement in a phenomenological context. In any case, the spray penetration model used in the current entrainment model only affects overall entrainment indirectly (via θ_{ch}) compared with the entrainment constant K, which is an important model parameter, as discussed below.

From the aforementioned scaling arguments, the total rate $dm_{tot\text{-}ent}/d\theta$ of unburned mass entrained into the spray must be directly proportional to the unburned-zone mass and inversely proportional to the characteristic entrainment time and can be written as

$$\frac{dm_{tot\text{-}ent}}{d\theta} \propto \frac{m_u}{\theta_{ch}} \tag{2}$$

Since the total unburned entrained mass is distributed among a total number of $I_{tot} \times J_{tot}$ packets, $dm_{tot\text{-}ent}/d\theta$ is divided by $I_{tot} \times J_{tot}$. Also, proper stratification in mixture entrainment must be ensured in the direction normal to the spray axis and for packets injected later in the injection process. Finally, the decay of spray entrainment as the spray

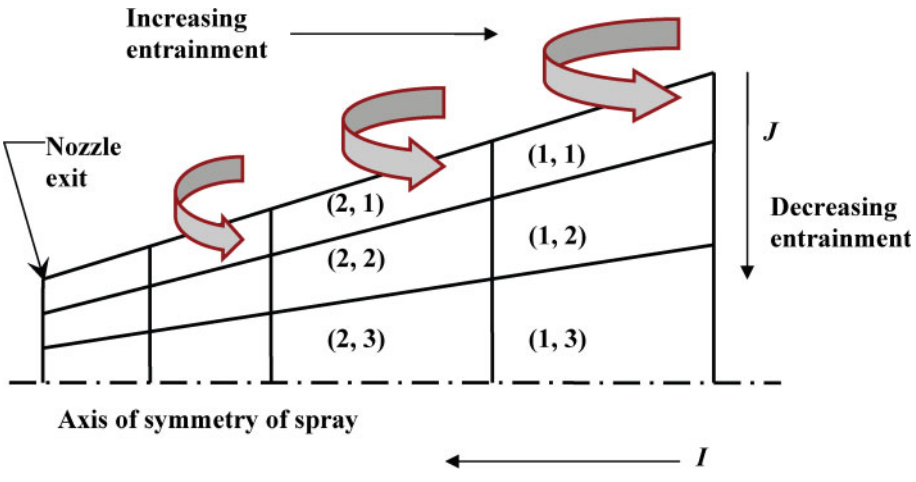

Fig. 2 Schematic diagram of packets classification showing spray entrainment and radial stratification

disintegrates and loses its initial momentum must be captured. Based on these considerations and following Bell [**35**], the mass m_{ent} of mixture entrained into any packet (I,J) in one calculation step $\Delta\theta$ is expressed as

$$m_{ent}(I,J) = K\frac{m_u}{I_{tot}J_{tot}(1+Y)}\frac{\Delta\theta}{\theta_{ch}}\exp\left(-\frac{I}{I_{tot}}\frac{J}{J_{tot}}\right) \quad (3)$$

where K is the entrainment constant, which is an important model parameter that influences the net spray momentum, Y is the ratio of time elapsed since the BOI to the total injection duration, and I_{tot} and J_{tot} are the maximum values of I and J respectively. The exponential term in equation (3) accounts for stratification of entrainment across the spray and progressively lower entrainment in packets that are injected later in the injection process (higher I values). The term $1+Y$ ensures that the overall rate of mixture entrainment in the spray decreases with increasing elapsed time since the BOI. This mimics reality because, as the spray penetrates into the surroundings, its velocity decreases and eventually mixture entrainment into the spray decreases.

4.3.2 *Diesel evaporation model*

The total amount of pilot diesel fuel is initially divided equally between all the packets, which are tracked separately thereafter. However, only evaporated diesel is allowed to enter the packets. All fuel droplets are initialized with the same initial user-specified Sauter mean diameter (SMD). Following Kanury [**36**], the droplet evaporation rates are calculated using a quasi-steady isolated droplet evaporation model in which the evaporation rates adjust instantly to the temperature and species concentration changes. At the end of each time step, the droplet diameters in each packet are updated on the basis of the remaining liquid volumes.

4.3.3 *Ignition model*

In pilot-ignited natural-gas engines, diesel fuel ignites first and then initiates natural-gas combustion. In this model, diesel ignition is modelled in the packets. Although natural gas may take part in the diesel ignition process [**6**], its specific effects are not very well known and, hence, are not considered here. Empirical Arrhenius-type ignition delay correlations, which were originally developed for predicting the ignition delays in conventional diesel combustion, greatly underpredicted the ignition delays for early BOIs in ALPING combustion [**37**, **38**]. Therefore, the Shell autoignition model [**39**] was used to model ignition in each packet. The Shell model employs generic species in a global eight-step chain-branching reaction mechanism of hydrocarbon ignition and includes the reactions for chain initiation, propagation, branching, and termination. The original model coefficients for fuel with a research octane number (RON) of 90 (assuming *n*-dodecane stoichiometry) were used with the exception of the pre-exponential factor A_{p3} controlling fuel consumption in the propagation cycle, which was modified from the original value of 1×10^{13} to 8×10^{11} to provide better ignition delay predictions [**37**].

Pre-ignition energy release, which is predicted in the ignition model, raises the packet temperatures, and ignition of a packet is assumed to occur when either the packet temperature exceeds 1100 K or the rate of increase in the packet temperature exceeds 10^7 K/s. These two conditions have been used by several researchers, including Halstead *et al.* [**39**]. In addition to these ignition criteria, it is reasonable to expect ignition to occur only if the equivalence ratio in each packet is within ignition limits. As observed by Sazhina *et al.* [**40**], artificial enforcement of ignition limits is necessary since the Shell model does not explicitly account for such limits. Therefore, in the present work, a packet is assumed to ignite if it satisfies *either* of the aforementioned temperature criteria *and* its equivalence ratio is within the assumed rich ignition and lean ignition limits of $\phi = 3$ and $\phi = 0.2$ respectively. Upon ignition, the Shell ignition model is deactivated for the packet and the packet combustion model is triggered.

4.3.4 *Packet combustion model*

After a packet ignites, diesel is allowed to burn according to the single-step global reaction mechanism adapted from Westbrook and Dryer [**41**], which is given by

$$\dot{m}_{d\text{-}ij} = A_{pd}\exp\left(\frac{-E_A}{RT_{ij}}\right)[C_{12}H_{26}]_{ij}^{0.25}[O_2]_{ij}^{1.5}\frac{V_{ij}\,MW_d}{\omega} \quad (4)$$

where $\dot{m}_{d\text{-}ij}$ is the diesel reaction rate (g/rad) in packet (I,J), the pre-exponential factor A_{pd} is assumed to be 2.5×10^{10} $(mol/cm^3)^{-0.75}/s$ (following trends in reference [**41**], this is lower than the value of 3.8×10^{10} recommended for decane), the activation energy E_A is 30 kcal/mol, $[C_{12}H_{26}]_{ij}$ is the packet diesel (*n*-dodecane) vapour concentration (mol/cm^3),

$[O_2]_{ij}$ is the packet oxygen concentration (mol/cm^3), T_{ij} is the packet temperature (K), V_{ij} is the instantaneous packet volume (cm^3), R is the universal gas constant (kcal/mol K), MW_d is the molecular weight of n-dodecane, and ω is the crankshaft angular velocity (rad/s). From equation (4), it is obvious that, for a given packet temperature, the diesel reaction rate will increase when either the fuel or oxygen concentration is increased. As the BOI is advanced from 20° before TDC to 60° before TDC, progressively higher levels of oxygen entrainment in packets are allowed because of longer ignition delays, thereby increasing the reaction rates and heat release rates without limits. In contrast with the behaviour of equation (4), the experimental peak heat release rates at advanced BOIs were found to be lower than at intermediate BOIs (e.g. 35–40° before TDC). This may be expected because the diesel pilot, when allowed to mix with the lean natural-gas–air mixture over a long ignition delay period, will probably be very lean in some spatial locations, thereby decreasing the local reaction rates. To capture these trends, equation (4) was modified only for lean packet equivalence ratios as

$$\dot{m}_{\text{d-}ij} = A_{\text{pd}} \exp\left(\frac{-E_A}{RT_{ij}}\right)[C_{12}H_{26}]_{ij}^{0.25}[O_2]_{ij}^{1.5} \times \frac{V_{ij}\,MW_d}{\omega}\left(1-\left|1-\phi_{ij}\right|^{C_\phi}\right) \quad (5)$$

where ϕ_{ij} ($\leqslant 1$) is the total equivalence ratio of packet (I,J) considering both diesel and natural gas, and the lean packet equivalence ratio exponent C_ϕ is set equal to 0.2.

Similar to packet diesel combustion, natural gas (methane) entrained into each packet together with air is assumed to burn according to the single-step global reaction mechanism [**41**]

$$\dot{m}_{\text{ng-}ij} = A_{\text{png}} \exp\left(\frac{-E_A}{RT_{ij}}\right)[CH_4]_{ij}^{-0.3}[O_2]_{ij}^{1.3} \times \frac{V_{ij}\,MW_{ng}}{\omega} \quad (6)$$

where $\dot{m}_{\text{ng-}ij}$ is the natural gas reaction rate (g/rad) in packet (I,J), $A_{\text{png}} = 8.3\times10^5\,\text{s}^{-1}$, and $E_A = 30$ kcal/mol. Also, to be consistent with the diesel reaction rate expression given in equation (5), the natural-gas reaction rate was modified only for lean total packet equivalence ratios as

$$\dot{m}_{\text{ng-}ij} = A_{\text{png}} \exp\left(\frac{-E_A}{RT_{ij}}\right)[CH_4]_{ij}^{-0.3}[O_2]_{ij}^{1.3} \times \frac{V_{ij}\,MW_{ng}}{\omega}\left(1-\left|1-\phi_{ij}\right|^{C_\phi}\right) \quad (7)$$

where ϕ_{ij} and C_ϕ have the same values as in equation (5).

The actual diesel and natural-gas burn rates are taken to be the lower of two rates: the rates at which they become available (by evaporation or entrainment) in the packet or the burn rates predicted by equations (4) to (7). The heat release rates in all ignited packets are determined as the product of the actual fuel mass burning rates and their respective lower heating values.

4.4 Flame zone

The flame zone, which models flame propagation in the natural-gas–air mixture, is formed when ignition first occurs in any packet and ceases to exist at the EOC. Conceptually, the flame zone refers to the combustion zones surrounding the ignited packets. Since spatially distributed combustion zones cannot be handled separately in a quasi-dimensional combustion model, these zones are lumped into a single 'flame zone'. Unlike traditional SI engine combustion, ALPING combustion does not originate from a single location inside the cylinder. Consequently, the computation of the flame area is challenging, and geometric modelling of the flame area as one spherical flame front (cf. reference [**42**]) with a single point of origin (e.g. a spark plug) is neither realistic nor feasible. Therefore, the flame area is treated in a rather unique way (based on the packet areas) in this paper, as explained later.

To model natural-gas combustion by premixed turbulent flame propagation, the entrainment and burn-up model of Tabaczynski *et al.* [**43**] is adopted. In this model, the small-scale turbulence structure model proposed by Tennekes [**44**] is used. Small-scale turbulence is described as 'vortex tubes' of diameter η (the Kolmogorov microscale) that are stretched by eddies of size λ (the Taylor scale). The main combustion implications of the Tennekes model are slow burning at the laminar burning velocity in the λ-scale regions and fast burning in the η-scale regions. The Tennekes model has previously been implemented and validated by Tabaczynski *et al.* [**43**] and further refined by Tabaczynski *et al.* [**45**] to simulate turbulent flame propagation in SI engines. With this model, the mass entrainment rate

$\dot{m}_e$ in the flame zone can be expressed as

$$\dot{m}_e = (\rho_u \rho_f)^{1/2} A_f u_e \tag{8}$$

where ρ_u is the unburned-zone density, ρ_f is the flame-zone density, A_f is the instantaneous mean flame area, and u_e is the turbulent entrainment velocity. Since equation (8) does not have an explicit dependence of the entrainment rate on the available unburned mass, flame entrainment remains inordinately large even near the EOC when the unburned-zone mass becomes very small. To overcome this issue, equation (8) was modified to account explicitly for the reduced availability of unburned mass towards the EOC, and the mass entrainment rate in the flame was calculated as

$$\dot{m}_e = (\rho_u \rho_f)^{1/2} A_f u_e \left[1 - \exp\left(\frac{-m_u}{c_{fdrop} m_{tot}}\right)\right] \tag{9}$$

where the exponential term ensures that the entrainment rate decreases exponentially as the unburned mass fraction m_u/m_{tot} in the cylinder decreases below a critical value that is dependent on the model constant c_{fdrop}. The value of c_{fdrop} was set to 0.0625 to ensure that the entrainment rate tapers off smoothly when more than 90 per cent of the unburned mixture has been entrained.

To evaluate the flame entrainment rate from equation (9), both A_f and u_e need to be determined. In ALPING combustion, several non-stationary distributed ignition centres are probable, resulting in many localized flamelets that may eventually interact with each other to form a single turbulent flame or may retain their individuality throughout the combustion process. Therefore, A_f should be calculated while accounting for the possible presence of multiple ignition centres. Also, increasing the number of ignition centres should lead to a larger enflamed area and faster combustion rates. Accordingly, the instantaneous mean flame area is assumed to be the envelope of the instantaneous enflamed area of ignited packets. For simplicity, each packet is presumed to retain its individuality throughout the combustion process, i.e. no interaction, which may lead to overlapping or combining of enflamed areas is allowed between the packets. The instantaneous flame area is then determined from the enflamed area of the ignited packets as

$$A_f = K_{Af} \sum_{n=1}^{n_{pign}} y_{pb}^{C_b} V_p^{2/3} \tag{10}$$

In equation (10), the proportionality constant K_{Af} (set to 0.9) and the burned mass fraction exponent C_b (set to 0.4) are model parameters. The number of ignited packets at any CA is n_{pign}, the packet burned mass fraction is y_{pb}, and the packet volume is V_p. Based on dimensional considerations, the packet area may be related to its volume raised to the two-thirds power; this relationship between the area and the volume has been used previously for heat transfer area calculations by Bell [**35**] and Krishnan [**46**].

The turbulent entrainment velocity u_e, which can be interpreted as the speed of propagation of ignition centres into the unburned gas, is determined from the equation

$$u_e = S_L + C_1 \left(\frac{\rho_u}{\rho_f}\right)^{1/2} u' \left[1 - \exp\left(\frac{-R_f}{C_2 L}\right)\right] \tag{11}$$

where S_L is the laminar burning velocity evaluated at instantaneous in-cylinder conditions, u' is the turbulence intensity, R_f is the equivalent spherical radius of the flame calculated from A_f, and L is the integral length scale. To find u_e, S_L is determined using a typical correlation for methane–air mixtures [**47**]. The values of C_1 and C_2 are 4 and 1 respectively. The exponential term in equation (11), which has been used before in SI combustion modelling [**48**, **49**], has been included to account explicitly for the increased importance of the turbulence intensity (relative to the laminar burning velocity) with increasing flame size. The initial value of L at the SOC is proportional to the instantaneous combustion chamber height with the proportionality constant C_4 set to 0.2, following Hill [**50**]. The initial value of u' at the SOC is assumed to be proportional to the mean piston speed with the proportionality constant $C_{u'}$ equal to 0.6. The values of L and u' at any subsequent time step are determined by assuming angular momentum conservation for individual eddies during rapid compression or expansion (rapid distortion theory) following reference [**43**], according to

$$L = L_i \left(\frac{\rho_{ui}}{\rho_u}\right)^{1/3} \tag{12}$$

$$u' = u'_i \left(\frac{\rho_u}{\rho_{ui}}\right)^{1/3} \tag{13}$$

where the subscript i refers to the initial values of the respective variables.

The turbulent mass burn rate $\dot{m}_b$ is proportional to the total unburned mass (total entrained mass – total burned mass) in the flame zone and is determined from the equation

$$\dot{m}_b = \frac{m_{etot} - m_{btot}}{\tau_b} + \rho_u A_f S_L \quad (14)$$

where m_{etot} is the cumulative mass entrained into the flame zone, m_{btot} is the cumulative mass burned in the flame zone, and τ_b is the characteristic burn time, which is determined as

$$\tau_b = \frac{C_3 \lambda}{S_L} \quad (15)$$

The burn time represents the characteristic time taken for laminar burning to occur in a length scale corresponding to the Taylor scale λ. The constant C_3 was assigned a value of 2.5 following reference [**48**]. Assuming isotropic turbulence, λ is calculated from the expression [**51**]

$$\frac{\lambda}{L} = \left(\frac{15}{A}\right)^{1/2} \left(\frac{u'L}{\nu}\right)^{-1/2} \quad (16)$$

where the constant A is set equal to 1, ν ($= \mu/\rho_f$) is the kinematic viscosity, and the dynamic viscosity μ is determined from the expression $\mu = 3.3 \times 10^{-7}\ T_f^{0.7}$ given in reference [**52**].

The flame zone heat release rate is evaluated as the product of the mass burn rate and the lower heating value of methane. The mass burned in the flame zone in one time step is transferred to the burned zone in the subsequent time step.

4.5 Burned zone

The burned zone is formed one time step after the SOC and contains burned products transferred every time step from the flame zone. The burned products in a packet are not transferred to the burned zone until the following conditions are satisfied: first, the packet temperature is lower than a critical temperature (1900 K), below which NO_x formation rates will become negligible, *and*, second, *either* more than 90 per cent of diesel and natural gas in a packet have burned *or* their reaction rates have become less than 1 per cent of their maximum values.

When both the first condition and the second condition are satisfied, all packet contents are allowed to mix instantaneously and adiabatically with the burned zone. This mixing process (termed 'dumping') is expected to capture hot regions of burned products in packets, which lead to most of the NO_x formed during combustion. When all packets are dumped, the flame area becomes zero, the flame zone ceases to exist, and combustion is terminated.

4.6 Heat transfer model

The overall heat transfer rate $dQ_{tot}/d\theta$ from cylinder gases to cylinder walls is determined using the Woschni [**53**] heat transfer correlation and the average cylinder temperature T_{avg}. Following reference [**35**], the heat transfer rate $dQ_i/d\theta$ from each zone i is obtained by weighting $dQ_{tot}/d\theta$ with the area (computed as volume raised to the two-thirds power) and temperature T_i of that zone according to

$$\frac{dQ_i}{d\theta} = \frac{dQ_{tot}}{d\theta} \frac{V_i^{2/3}(T_i - T_{wall})}{\sum_i V_i^{2/3}(T_i - T_{wall})} \quad (17)$$

where V_i is the zone volume and T_{wall} is the cylinder wall temperature (set equal to 480 K).

5 RESULTS AND DISCUSSION

In this section, predictions from the phenomenological simulation are compared with experimental results at different BOIs for ALPING combustion. The engine details and operating conditions (used as model inputs) are given in Table 1. A 2.4 l single-cylinder research engine equipped with a dedicated pilot injection system was used for the ALPING experiments. The diesel injected quantity was fixed at 3.3 g/min (the minimum value possible with the injection system) for all BOIs to ensure minimal NO_x

Table 1 Engine details and operating conditions

Parameter	Specification
Engine type	Single cylinder, four stroke
Bore (mm)	137
Stroke (mm)	165
Compression ratio	14.5
Combustion system	Direct injection, Mexican hat
Diesel injection system	Electronic, common rail
Diesel injector	Pencil type, four holes
BOI	Variable (20–60° before TDC)
Diesel injection pressure (bar)	359.5
Diesel injected quantity (g/min)	3.3
Diesel injection duration (deg CA)	5
Natural-gas fuelling rate (g/min)	77.3–94.0 (variable with BOI)
Engine speed (r/min)	1700
Experimental BMEP associated with fuelling rates (bar)	6
Intake manifold pressure (kPa)	181
Intake manifold temperature (K)	348

emissions. However, natural-gas fuelling was varied to maintain a BMEP of 6 bar for all BOIs at a constant speed of 1700 r/min. The intake manifold pressure and the temperature were fixed at 181 kPa and 348 K respectively. All the model parameters were calibrated (see reference [**38**] for details) for a baseline test case (the 40° before TDC BOI) and systematic model sensitivity studies were performed to obtain optimal values (Table 2). *Subsequently, all model parameters (except J_{tot} as discussed below) were held constant for all other experimental conditions (different BOIs) discussed in this paper*. The simulation was first validated with experimental pressure and heat release histories over the entire range of BOIs from 20° before TDC to 60° before TDC. Then, model predictions at the early BOI of 60° before TDC were examined closely. Finally, parametric studies were performed at the early BOI of 60° before TDC with different intake charge temperatures, pilot fuel quantities, and natural-gas equivalence ratios.

5.1 Model validation at various BOIs

Before discussing the model validation results, it is important to clarify the extent to which model predictions can be expected to match experimental results. While it is relatively straightforward to predict the cylinder pressures (since the cylinder pressure is an average global quantity), the predicted heat release rates are profoundly influenced by local (packet) reaction rates. Since the experimental heat release rates are determined using a two-zone combustion model [**46**], they are dependent on the first derivative of the measured cylinder pressure. Therefore, in this sense, both predicted and experimentally derived heat release rates are 'differentiated' quantities that are dependent either on local packet conditions or on the pressure derivative, while cylinder pressures are 'integrated global' quantities. Therefore, while comparing the experimental and predicted heat release rates throughout this paper, it is important to remember that, although the cylinder pressures may be predicted satisfactorily, a perfect match between the heat release rates may not exist. In fact, some differences may be expected in the heat release histories because of the fundamental differences between the combustion models used in the simulation and the experimental heat release analysis and their associated assumptions and limitations. The difficulties in matching the experimental and simulated heat release and the accuracy to which the heat release histories can be predicted were also discussed by Hountalas *et al.* [**54**] for diesel engines.

Table 2 Model parameter values

Parameter	Value
Computational time step $\Delta\theta$ (deg CA)	1/32
Entrainment constant K	0.05
Pre-exponential factor A_{pd} in diesel reaction rate ((mol/cm^3)$^{-0.75}$/s)	2.5×10^{10}
Lean packet equivalence ratio exponent C_ϕ	0.2
Flame area proportionality constant K_{Af}	0.9
Turbulent entrainment velocity constant C_1	4.0
Turbulent entrainment velocity constant C_2	1.0
Characteristic burn time proportionality constant C_3	2.5
Integral length scale proportionality constant C_4	0.2
Flame zone entrainment drop constant C_{fdrop}	0.0625
Turbulence intensity proportionality constant $C_{u'}$	0.6
Packet burned mass fraction exponent for flame area calculations C_b	0.4
Total number I_{tot} of I packets	41
Total number J_{tot} of J packets	3–12
Initial diesel droplet diameter (SMD) (μm)	30
Shell model constant A_{p3} for a primary reference fuel of RON 90	8×10^{11}

5.1.1 Ignition delay behaviour

In the early stages of model development, it was determined that predicting the onset of ignition over a wide range of BOIs is critically important to predict ALPING combustion accurately. Two different types of ignition model were originally considered [**38**]:

(a) Arrhenius-type ignition delay correlations (typically used in conventional dual-fuel combustion models);
(b) the Shell autoignition model.

The Arrhenius-type ignition delay correlations were unable to predict the experimental ignition delay trends satisfactorily and, consequently, the Shell model was adopted. The reader is referred to reference [**37**] for a detailed discussion of the shortcomings of Arrhenius-type ignition delay correlations and the need for the Shell model to predict pilot ignition in ALPING combustion.

Figure 3 shows the experimental and predicted ignition delays (with the Shell model) for different BOIs. To determine the experimental ignition delays, the CA-resolved cylinder pressure histories were measured using a Kistler model 7061B pressure transducer, and the experimental heat release rates were determined using the two-zone combustion model [**46**]. The pilot injection timings (BOIs) were determined using CA-resolved measurements from an injection pressure sensor mounted on the fuel injector body. The onset of ignition (SOC) was determined as the start of heat release (the CA when positive heat release rates were first observed), and

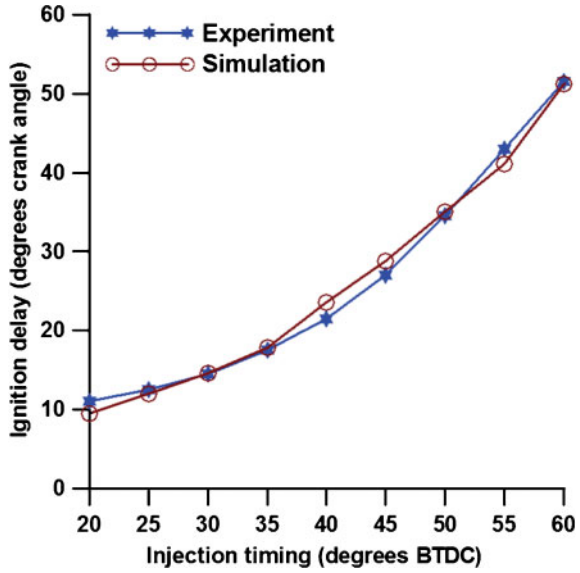

Fig. 3 Experimental and Shell-model-predicted ignition delays at different BOIs

the experimental ignition delay was defined as the difference between the BOI and the SOC. Figure 3 shows that the experimentally measured ignition delay increases with progressively earlier pilot injection. As the BOI is advanced, the in-cylinder temperatures at the time of injection are substantially lower, resulting in slower preignition reactions, longer ignition delay periods, and thus lower NO_x emissions. As is evident from Fig. 3, the predicted ignition delays match quite well the experimental values over the entire BOI range. It must be noted that these predictions were obtained with all original Shell model constants for a primary reference fuel of RON 90 except A_{p3}, which was modified to 8×10^{11} [**37**].

5.1.2 Heat release and combustion pressure histories

To achieve good combustion pressure and heat release predictions at all BOIs, many model parameters were simultaneously optimized during the calibration phase [**38**] to obtain the values given in Table 2. *Sensitivity studies showed a strong coupling between combustion in packets and flame combustion*. As the BOI is advanced, the injected diesel fuel will undergo better mixing over longer ignition delay periods and a greater number of ignition centres will be available throughout the combustion process. Based on this premise, it was decided that the total number of ignition centres (packets) should be increased with BOI advancement. Since greater diesel spray penetration and radial stratification are possible at early BOIs, J_{tot} is increased as the BOI is advanced to account for radial stratification of mixture entrainment.

Figure 4 shows the predicted (subscript sim) and experimental (subscript expt) pressures and heat release rates for different BOIs. For these results, all model parameters were fixed at the values specified in Table 2. The only parameter that was changed with the BOI was J_{tot}, whose specific value at each BOI is shown in the corresponding figure. In Fig. 4, slight discrepancies may be noted between some of the experimental and simulated pressure curves even before ignition. The primary experimental causes for these discrepancies were as follows:

(a) the long valve overlap period (about 45° CA) in the single-cylinder engine and the relatively late IVC (37° after bottom dead centre) that led to inaccuracies in the calculation of the total mass trapped inside the cylinder at IVC from the measured intake manifold conditions or flow-rates;
(b) the location of the cylinder pressure transducer, which was mounted via connecting passages to the combustion chamber (not flush mounted), owing to the lack of direct access ports in the cylinder head of the single-cylinder engine.

Although the model was calibrated [**38**] with motoring pressure traces, the best match still showed some discrepancies between measurements and predictions. These same discrepancies were also observed when the measured and predicted combustion pressure traces were compared.

For the late BOI of 20° before TDC, Fig. 4(a) shows that the predicted pressures match the measured pressures quite well but the peak heat release rate is underpredicted. While the SOC is predicted well, the peak heat release rates are underpredicted and the combustion rates are slower. The reason for slower combustion at the 20° before TDC BOI is evident when the packet equivalence ratios are examined closely. Figure 5 shows the packet equivalence ratio distributions at the SOC in terms of the percentage of packets that fall within a given range of equivalence ratios for five different BOIs. This representation (in terms of percentages) is necessary to compare the packet equivalence ratio distributions over the range of BOIs that use different total numbers of packets. In Fig. 5, a given packet equivalence ratio range value indicates the range between that value and the immediately higher equivalence ratio value; for example, an equivalence ratio range value of 0.6 signifies the equivalence ratio range 0.6–0.7.

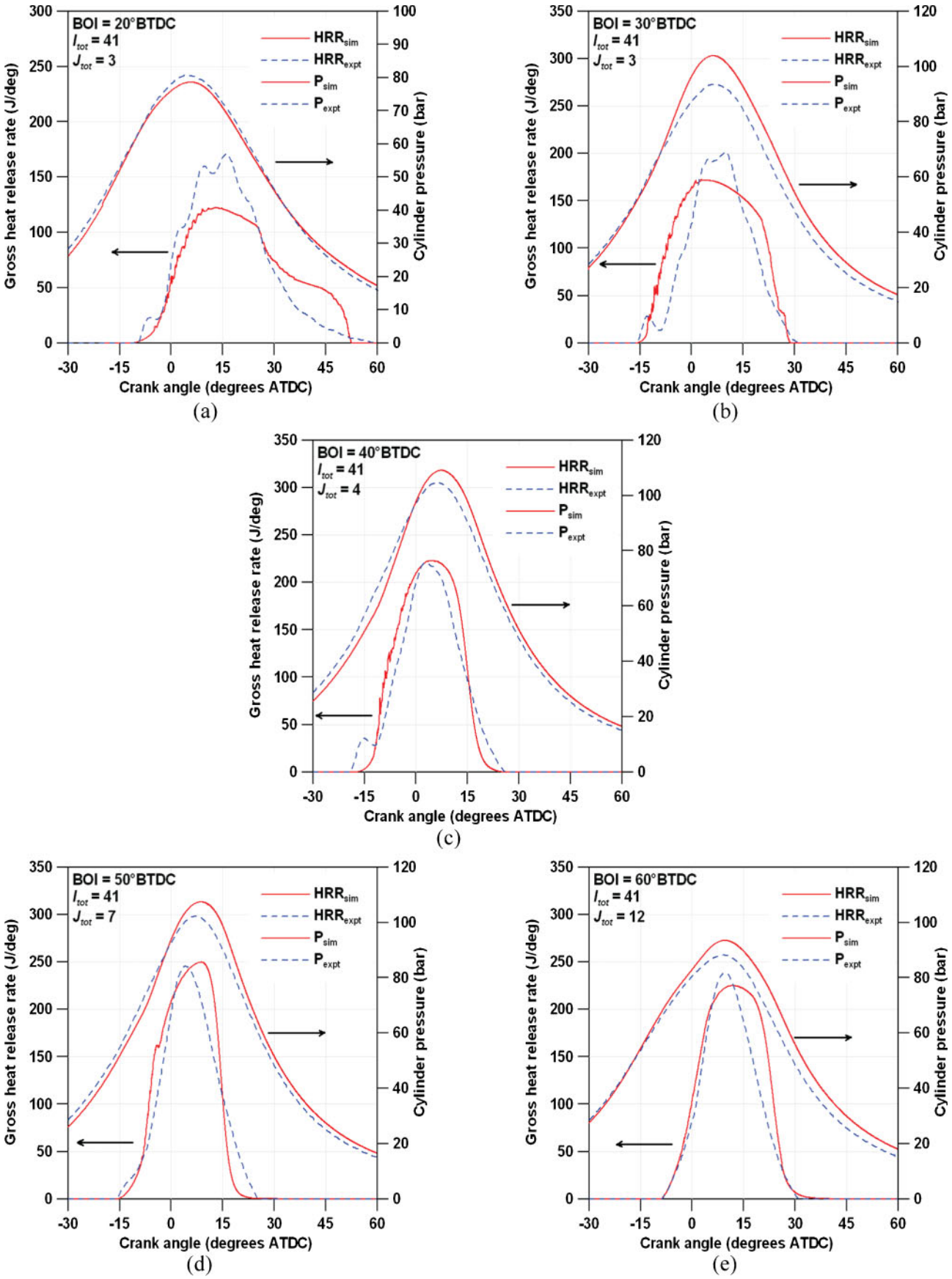

Fig. 4 Comparison of the experimental and predicted heat release rates (HRRs) and cylinder pressures *P* for different BOIs

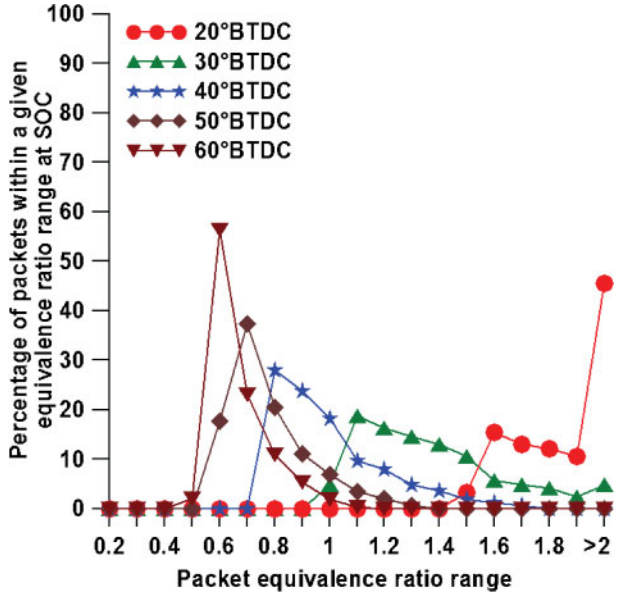

Fig. 5 Simulated results of packet equivalence ratio distributions at the SOC for different BOIs. Note that, in this figure, a packet equivalence ratio range of 0.6 (for example) represents the range 0.6–0.7

As is evident from Fig. 5, for the 20° before TDC BOI, all packets are richer than stoichiometric at the SOC, with nearly 50 per cent of the packets richer than the equivalence ratio of 2.0. Therefore, they exhibit slower heat release rates and, consequently, attain lower peak temperatures than for intermediate BOIs. Cooler packets reduce the effective flame area and lead to slower flame combustion, thus resulting in lower peak heat release rates. However, the overall heat release duration is predicted fairly well despite the overprediction of heat release rates towards the EOC for 20° before TDC.

As shown in Figs 4(b) and (c), the overall heat release rates are predicted better for the 30° before TDC and 40° before TDC BOIs than for the 20° before TDC BOI but the peak pressures are slightly overpredicted. The predicted heat release durations matched well the experimental durations for both 30° before TDC and 40° before TDC. For 30° before TDC, the peak pressures are overpredicted because the initial heat release rates are overpredicted. Compared with 20° before TDC, the packet equivalence ratios for 30° before TDC are closer to stoichiometric (see Fig. 5) and so the packet temperatures are much higher, leading to faster combustion rates. However, the peak heat release rates are still slightly underpredicted. On the other hand, for 40° before TDC, both the cylinder pressure and the heat release rate predictions are better. The peak heat release rates are predicted satisfactorily and the initial heat release rates are only slightly overpredicted. From Fig. 5, it may be observed that almost 70 per cent of the packets lie within the equivalence ratio range 0.8–1.1 for 40° before TDC. Therefore, the combustion rates are faster and the packet temperatures are also the highest for 40° before TDC. It must be noted that the J_{tot} value used for 40° before TDC is increased from 3 to 4 for the same I_{tot} value (of 41) as 30° before TDC to account for the higher number of potential ignition centres for the earlier BOI.

Figures 4(d) and (e) show model predictions for the early BOIs of 50° before TDC and 60° before TDC, which were obtained with J_{tot} values of 7 and 12 respectively. As mentioned before, one important objective of the simulation is to predict combustion at early BOIs, which yielded the best NO_x–efficiency trade-offs in the ALPING experiments. For 50° before TDC, both the heat release rates and the cylinder pressures are predicted very well. A slight delay in the occurrence of the peak heat release rate may be observed together with a slight underprediction of the heat release duration. The heat release prediction for 60° before TDC is even better. The model predicts the SOC, heat release duration, initial heat release rates, and peak heat release rates very well, with the only downside being a slight overprediction of the peak pressure for 60° before TDC. Overall, the predictions at early BOIs are much better than for late and intermediate BOIs, thus satisfying the main objective of the model development effort. It is also interesting to note that the experimental heat release profiles for the 50° before TDC and 60° before TDC BOIs do not exhibit the initial heat release peak that was visible for late and intermediate BOIs. Similarly, the heat release spikes that were noted in the predicted heat release curves for late and intermediate BOIs are virtually absent at 50° before TDC and 60° before TDC. For early BOIs, diesel has sufficient time to mix with the surrounding lean natural-gas–air mixture during the long ignition delay periods, and therefore it is possible that, upon ignition, pilot diesel combustion occurs simultaneously with natural-gas combustion by localized flame propagation. Consequently, there is no distinct initial heat release peak in the experimental heat release curves. In the simulation, the long ignition delay periods for 50° before TDC and 60° before TDC resulted in packet combustion at substantially leaner equivalence ratios (see Fig. 5), thus smoothing out the initial heat release spikes that were observed at late and intermediate BOIs. As observed in Fig. 5, a majority of packets for the 50° before TDC BOI and virtually all packets for 60° before TDC were leaner than

stoichiometric at the SOC, with almost 60 per cent of packets lying in the 0.6–0.7 equivalence ratio range at the SOC for 60° before TDC. These lean packets led to lower peak packet temperatures at early BOIs, as described in the next section.

5.1.3 *Peak packet temperatures*

Since NO_x formation is exponentially dependent on the local temperatures in any combustion process, it is useful to examine the packet temperatures to understand the potential for NO_x formation at different BOIs. Flynn *et al.* [**10**] established that local temperatures higher than approximately 2000 K will invariably lead to unacceptable levels of engine-out NO_x emissions; therefore, it is important to keep local temperatures below 2000 K to achieve LTC.

The simulated packet temperature trends are illustrated in Fig. 6, which shows the percentages of packets that fall within a given peak packet temperature range for different BOIs. Again, this representation (in terms of percentages) is necessary because different BOIs use different total numbers of packets. In Fig. 6, a given peak packet temperature range value indicates the temperature range between that value and the immediately preceding temperature value (lower by 100 K); for example, a peak packet temperature range value of 2600 K signifies the temperature range 2500–2600 K. Figure 7 shows the average peak packet temperatures

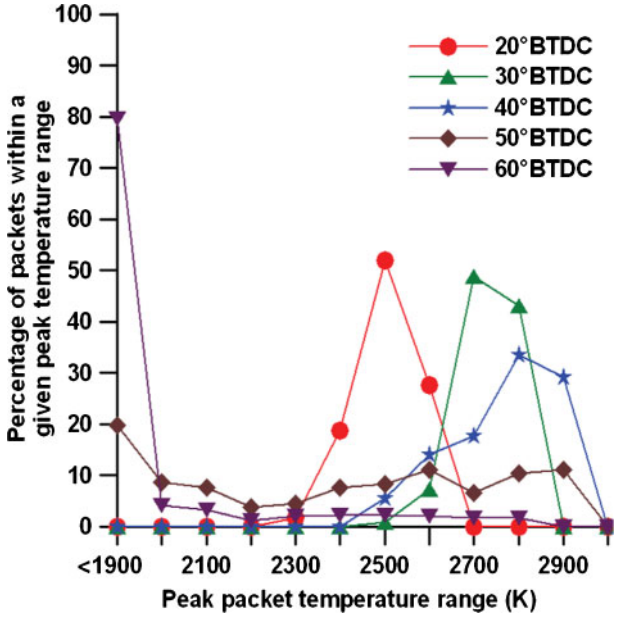

Fig. 6 Simulated results of the peak packet temperature distributions for different BOIs. Note that, in this figure, a temperature range of 2000 K (for example) represents the range 1900–2000 K

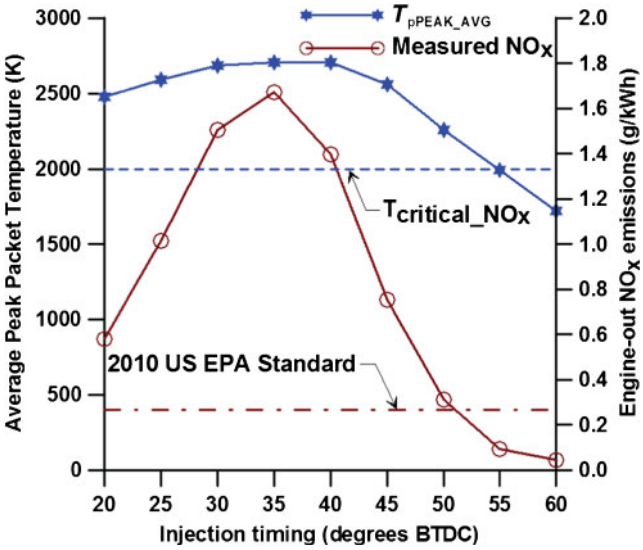

Fig. 7 Average peak packet temperatures (simulated) and engine-out NO_x emissions (measured) for different BOIs

T_{pPEAK_AVG} and the experimentally measured engine-out NO_x emissions at different BOIs. For each BOI, the maximum (peak) temperature attained by each packet over its individual lifetime (from the BOI until the EOC) was stored in an array. For a given number of packets, the numerical average of all these peak packet temperatures was computed and designated as the average peak packet temperature T_{pPEAK_AVG}. Consequently, T_{pPEAK_AVG} is not simply an average zone temperature but the average of the peak temperatures of packets (which were usually the hottest regions in the cylinder, routinely exceeding 2000 K), which are probably more important for NO_x formation. For reference, the critical temperature ($T_{critical\_NO_x} \approx 2000$ K) at which NO_x formation becomes significant and the 2010 US Environmental Protection Agency (EPA) NO_x emissions standard of 0.27 g/kW h for heavy-duty diesel engines are also shown in Fig. 7.

In addition to the high local in-cylinder temperatures, NO_x formation is also dependent on the residence times of these high-temperature regions. To illustrate the relative importance of the residence times of the high-temperature regions, Fig. 8 presents the peak packet temperatures and the corresponding normalized packet combustion durations (representing the in-cylinder residence times of hot regions) for all packets at different BOIs. In this figure, the actual combustion duration (from the SOC until the EOC) for each ignited packet was normalized with respect to the overall combustion duration for a given BOI to obtain the normalized packet combustion duration. In interpreting Fig. 8, it is important to note that the peak temperatures of

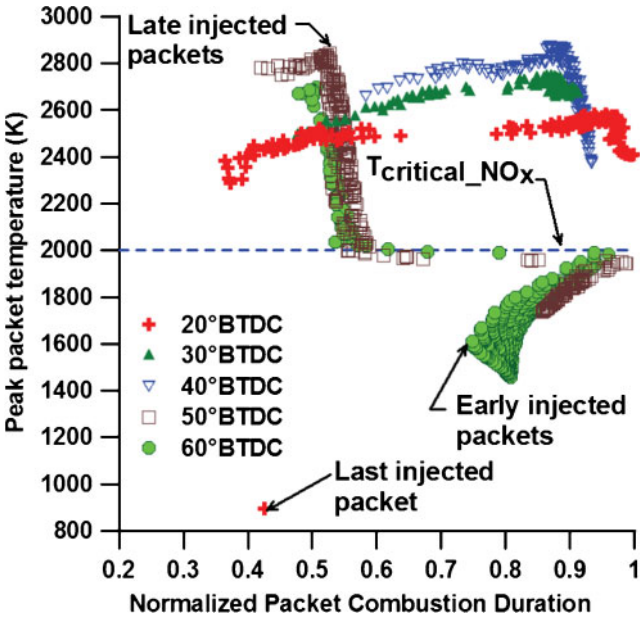

Fig. 8 Peak packet temperatures and corresponding normalized packet combustion durations (effective packet residence times) at different BOIs. Note that the combustion duration for each packet was normalized with the overall combustion duration at a given BOI

the flame zone were much lower (about 1600–1700 K) at all BOIs and the normalized flame residence times were 1.0 (by definition).

From Fig. 6, it is evident that 80 per cent of packets for the 60° before TDC BOI had peak temperatures below 1900 K; this is also reflected in Fig. 7 where 60° before TDC showed a $T_{\text{pPEAK\_AVG}}$ value of 1720 K. In Fig. 8, the peak packet temperatures and the normalized combustion durations for all packets at the 60° before TDC BOI are shown. For this early BOI, most packets (especially the packets that were injected earlier in the pilot injection process) experienced peak temperatures significantly lower than 2000 K and relatively long normalized combustion durations (0.7–0.95). Only a small fraction of packets (mostly injected later in the pilot injection process) attained higher peak temperatures but shorter normalized combustion durations (0.5–0.6). In general, most of the packets for the 60° before TDC BOI attained low peak temperatures (because these packets were very lean even at the SOC, as observed in Fig. 5) and persisted for most of the combustion duration. These predictions are consistent with the extremely low NO_x emissions measured for 60° before TDC. On the other hand, even though 20 per cent of packets at 50° before TDC had peak temperatures lower than 1900 K and long normalized combustion durations (0.85–1.0), the engine-out NO_x emissions were relatively higher because the remaining peak packet temperatures were distributed throughout the temperature range and several packets were at or near stoichiometric conditions at the SOC. Since more than 70 per cent of the packets attained peak temperatures higher than 2000 K, and about 10 per cent of the packets fell in the range 2800–2900 K, $T_{\text{pPEAK\_AVG}}$ was much higher at 2260 K.

As observed in Fig. 7, the highest NO_x emissions were measured in the BOI range 30–40° before TDC, indicating the highest local temperatures at these conditions. This is confirmed in the simulated peak temperature and normalized combustion duration trends (see Fig. 8) for the 40° before TDC BOI, for which nearly 60 per cent of the peak packet temperatures fell between 2700 K and 2900 K and their normalized combustion durations were between 0.55 and 0.9. Also, the highest $T_{\text{pPEAK\_AVG}}$ values of about 2700 K were obtained for the 35° before TDC and 40° before TDC BOIs. For the late BOI of 20° before TDC, more than 98 per cent of the predicted peak packet temperatures were between 2300 K and 2600 K, leading to a much higher $T_{\text{pPEAK\_AVG}}$ value of about 2480 K compared with the early BOI of 60° before TDC. Virtually all packets for the 20° before TDC BOI attained peak temperatures higher than 2000 K and normalized combustion durations between 0.35 and 1.0; the only exception was the last injected packet in the interior regions of the spray (see Fig. 8), which had a very low peak temperature of about 900 K and a residence time of only 0.4. The relatively higher peak packet temperatures and the corresponding wide range of packet residence times for the 20° before TDC BOI explain the significantly higher engine-out NO_x emissions measured for 20° before TDC than for 60° before TDC. More importantly, these observations confirm a *strong correlation between the peak local (packet) temperatures, their effective residence times (the normalized packet combustion durations), and the measured NO_x emissions for all BOIs in ALPING combustion*. In particular, if the average peak local (packet) temperature exceeded the critical NO_x formation temperature of 2000 K for any BOI and the packet residence times were comparable with the overall combustion durations (normalized durations longer than 0.5), the measured engine-out NO_x emissions were always higher than the 2010 US EPA NO_x standard for heavy-duty diesel engines.

5.1.4 *Detailed results at the early BOI of 60° before TDC*

Since the lowest NO_x emissions were obtained at the early BOI of 60° before TDC, it is instructive to

examine model predictions at this BOI in greater detail. The zonewise heat release rates and cumulative heat release fractions are illustrated in Figs 9(a) and (b) respectively. In these figures, the subscripts p, f, and b refer to the packets, flame, and burned zones respectively, the subscripts d and ng refer to diesel and natural gas respectively, and the subscript tot refers to the total heat release in the cylinder. The cumulative heat release fractions were calculated as ratios of cumulative heat release occurring in different zones to the total fuel chemical energy input from both diesel and natural gas. Most of the combustion heat release (approximately 87 per cent) occurred in the flame zone, with packets contributing only about 4 per cent. Figure 9(a) shows that virtually all the packet heat release occurred early (between 10° before TDC and 10° after top dead centre (after TDC)) in the combustion process. The heat release in the packets increased their temperatures and led to rapid expansion of the packets, which in turn increased the effective flame area. Thus, the initial packet heat release rates exerted a profound influence on flame entrainment and burn rates through the flame area, thus affecting the flame zone heat release rates. Since the overall combustion heat release occurs for almost 40° CA, in contrast with much shorter combustion durations typically observed for HCCI-type combustion [**11**], ALPING combustion is clearly slower than HCCI and results in smoother pressure rise rates, thus enabling high-load (BMEP, about 12 bar) engine operation. In the packets, most of the heat release (about 3 per cent of the total fuel energy input) is due to diesel combustion and only 1 per cent arises from combustion of entrained natural gas. This is consistent with the actual experimental engine operating condition in which measured diesel flow corresponded to only about 3 per cent of the total fuel chemical energy input. Also, owing to the different combustion rates of diesel and natural gas in the packets, a delay between the onset of diesel and natural-gas heat release in the packets is observed.

Figure 10 shows the temperatures of different zones (the subscripts u, f, and b refer to the unburned, flame, and burned zones respectively), the average cylinder temperature T_{avg}, and the instantaneous maximum temperature $T_{inst\text{-}max}$ among all zones inside the cylinder. The flame and burned zones are formed only at the SOC and, after the EOC, the packets and the flame zone cease to exist. Therefore, T_b and T_f are zero before the SOC and T_f is zero after the EOC. The peak values of T_f and T_b are only about 1650 K. These relatively low

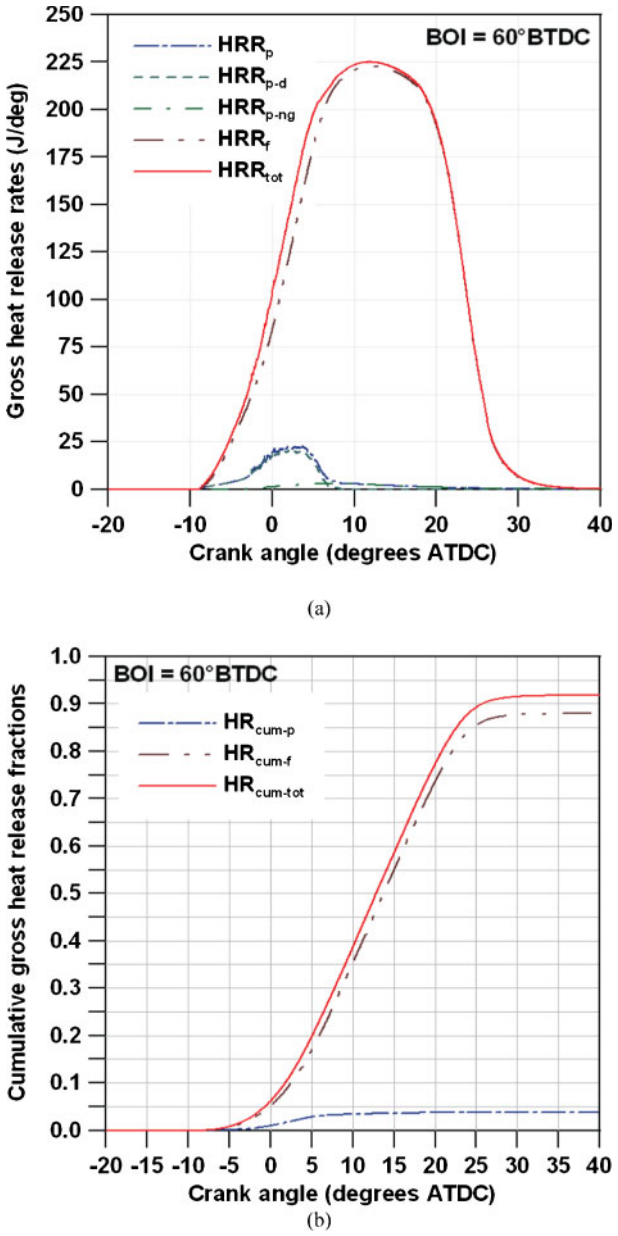

Fig. 9 (a) Zonewise heat release rates (HRR) and (b) cumulative heat release fractions (HR_{cum}) for the 60° before TDC BOI. The subscripts in this figure refer to various zones or fuels as follows: p, packets; p-d, packet diesel; p-ng, packet natural gas; f, flame; tot, total (all zones); cum-p, cumulative packets; cum-f, cumulative flame; cum-tot, cumulative total (all zones)

peak flame temperatures (the peak T_f value is very much less than $T_{critical\_NO_x}$) are due to the very lean equivalence ratio (approximately 0.38) of the flame zone. Consequently, very little NO_x will be formed in the flame zone. At the SOC, $T_{avg} = T_u$ but, later, T_{avg} increases until it becomes equal to T_b (towards the EOC) since most of the cylinder contents are burned. Compared with T_f and T_b, the peak value of $T_{inst\text{-}max}$

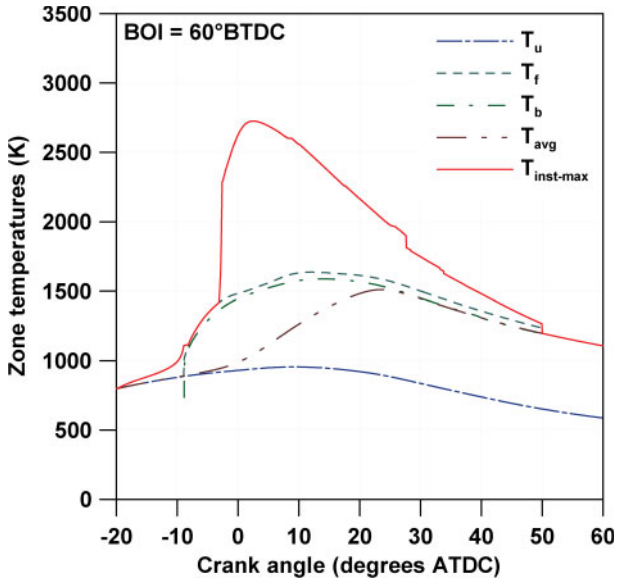

Fig. 10 Zonewise temperature profiles for the 60° before TDC BOI. The subscripts in this figure refer to various zone temperatures as follows: u, unburned zone; f, flame zone; b, burned zone; avg, average; inst-max, instantaneous maximum temperature in the cylinder

is much higher (greater than 2700 K) and is attained by only a few packets (less than 2 per cent, as shown in Fig. 5). After the initial stages of combustion (up to 5° before TDC) where $T_{\text{inst-max}}$ is only slightly higher than T_f, the hottest zones in the cylinder throughout the combustion process are the packets. Therefore, the simulation predicted that the diesel and natural-gas combustion processes in the packets (as opposed to the lean flame zone) are virtually the only source of NO_x formation in ALPING combustion.

Figure 11 provides additional results, indicating the important differences between the flame zone and combustion in the packets. Figure 11(a) shows the mass fraction histories of diesel and natural gas associated with all the packets in the cylinder. All diesel fractions shown here were obtained with respect to the total mass of diesel injected into the cylinder, while the natural-gas burned fraction was obtained with respect to the total mass of natural gas entrained in the packets throughout the combustion process. The entire diesel quantity is injected within 5° CA after the BOI. Diesel evaporation started at the BOI and, by the time that injection is over, about 30 per cent of diesel had evaporated. This is also reflected in the behaviour of the liquid diesel fraction with the maximum of about 70 per cent occurring at the EOI. The entire diesel evaporation process for the 60° before TDC BOI occurred within 20° CA after the BOI. Consequently, the physical component (fuel evaporation and mixing) of ignition delay was much shorter than the chemical component (pre-ignition reactions). After the SOC, the mass fraction of diesel burned in the packets increased rapidly and nearly 40 per cent of the injected diesel burned before TDC, with the entire diesel being consumed before 10° after TDC. Compared with the overall diesel burn duration of less than 20° CA, natural-gas combustion in the packets was much slower, persisting until about 30° after TDC. Only 25 per cent of the total natural gas entrained into the packets burned within the available time; the remaining unburned natural gas was transferred to the burned zone together with the dumped packets. Slower burning of natural gas (methane) in the packets is believed to occur for two important reasons: first, the self-inhibiting nature of methane oxidation; second, the non-inclusion of possible enhancement of methane burn rates in the packets due to local turbulence. The former cause is attributable to the chosen global kinetic scheme; i.e. the negative exponent (−0.3) for methane concentration in equations (6) and (7) inhibits reaction rates at high methane concentrations in the packets. On the other hand, modelling the potential enhancement of methane burn rates in the packets due to local turbulence is beyond the scope of the phenomenological framework adopted in the current simulation.

Figure 11(b) illustrates important flame zone behaviour including the flame zone entrainment and burn histories, the flame temperature T_f, and the total number n_{dump} of dumped packets at a given CA. The cumulative flame entrainment and burn histories clearly indicate that entrainment in the flame zone was faster than combustion of the entrained mass throughout the combustion process; in addition, only about 95 per cent of the entrained mass burned. The flame-zone burned mass fraction increased rapidly after the initial combustion phase (after TDC) and exhibited a fairly linear trend thereafter until near the EOC. The attainment of the EOC was triggered by the commencement of the dumping process (shown by the increase in n_{dump}) around 25° after TDC, which led to a decrease in the flame area because the dumped packets no longer contributed to the flame area computations. Owing to this decrease in the flame area after the start of dumping and the reduced availability of fresh natural-gas–air mixture in the unburned zone, the flame mass entrainment as well as the burn rate tapered off.

Figure 11(c) illustrates the peak packet temperatures as functions of the axial packet number I for different values of the radial stratification index J.

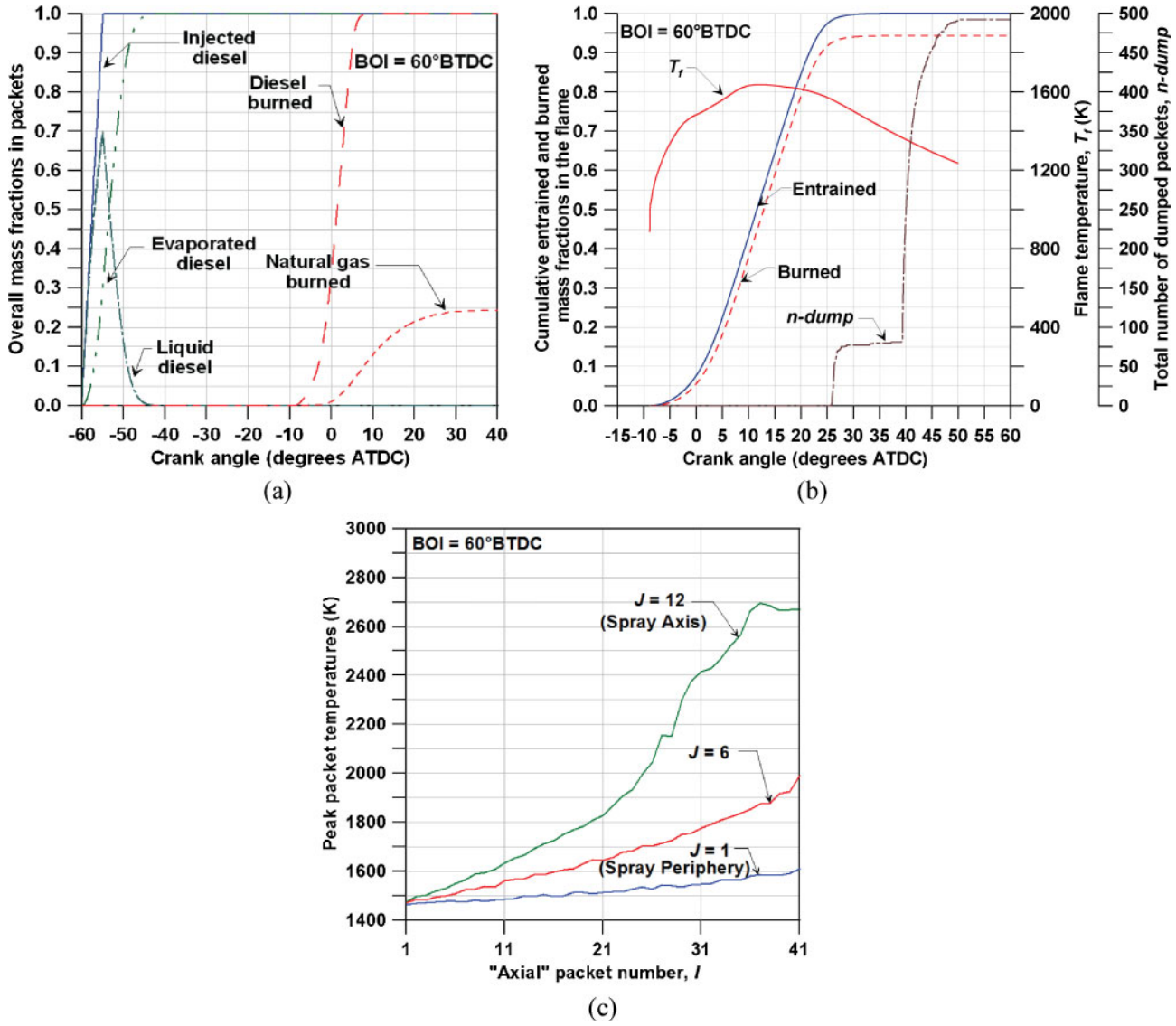

Fig. 11 Detailed results for the 60° before TDC BOI illustrating (a) the packet mass fractions, (b) the flame-zone mass fractions, flame temperature, and total number of dumped packets, and (c) the peak packet temperatures

The peak packet temperatures varied between 1500 K and 2700 K over the range of I and J values. For all J values, the peak packet temperatures increased with increasing I values, which represent packets injected later in the injection process. However, the magnitude of this increase was greater for higher J values, which represent packets that were nearer to the spray axis (e.g. $J = 12$). Interior packets that were also injected towards the end of the injection process experienced less entrainment and attained relatively higher equivalence ratios (closer to stoichiometric) than packets in the spray periphery (e.g. $J = 1$). Therefore, these interior packets experienced faster combustion rates and attained higher peak temperatures.

5.2 Parametric studies

In this section, the predictive capabilities of the phenomenological model are explored. The predicted effects of three important engine operating parameters including the intake charge temperature T_{in}, the pilot fuel quantity Q_{inj}, and the natural-gas equivalence ratio ϕ_{NG} on ALPING combustion are examined for the early BOI of 60° before TDC.

5.2.1 Intake charge temperature effects

Figure 12 illustrates the effects of T_{in} on the predicted cylinder pressure, heat release rate, and peak packet temperature for 60° before TDC. As T_{in} is increased

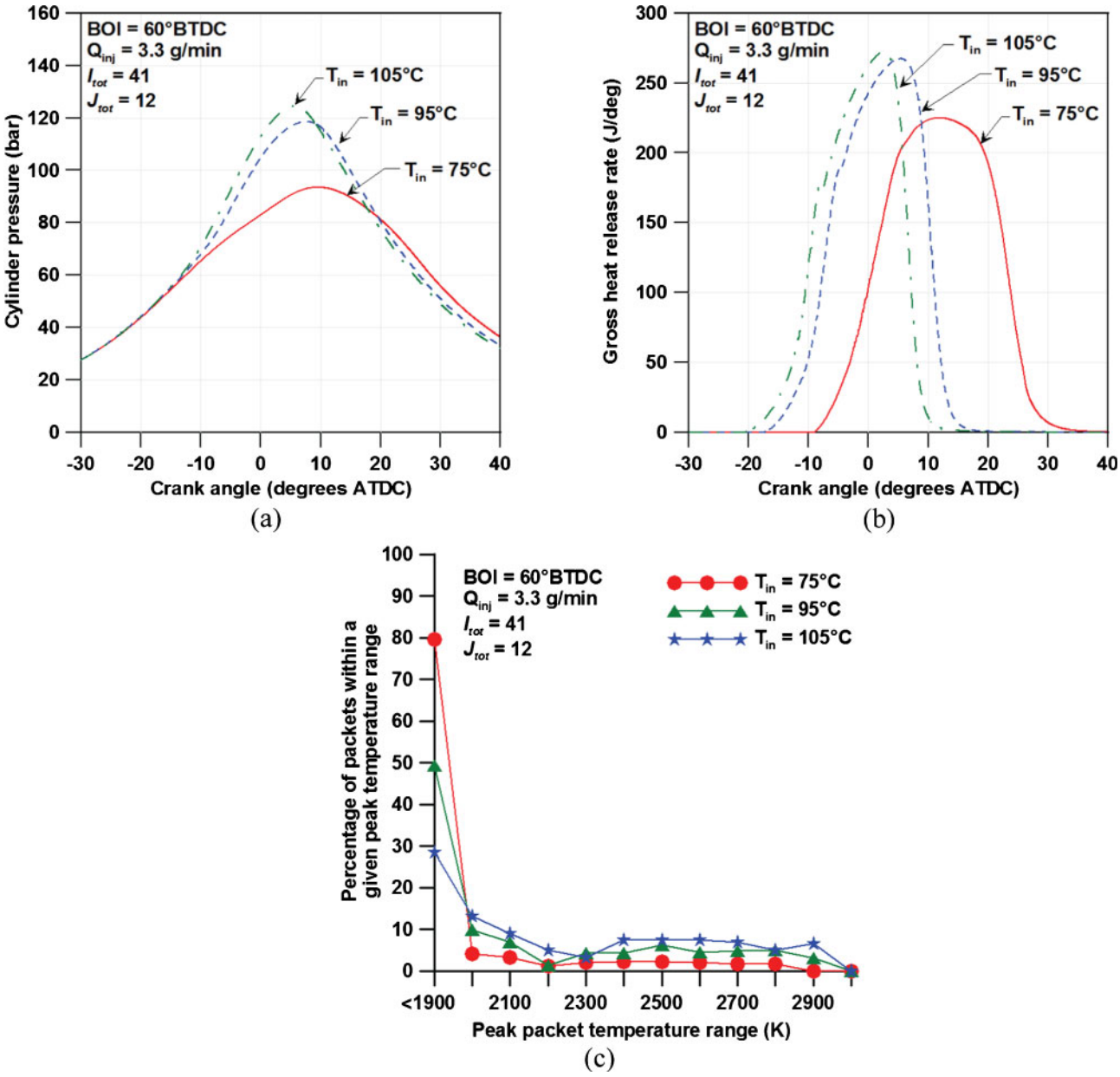

Fig. 12 Effects of the intake charge temperature T_{in} on (a) the predicted cylinder pressure, (b) the predicted heat release rate, and (c) the predicted peak packet temperature ranges for the 60° before TDC BOI

from 75 °C to 105 °C, the onset of ignition is progressively advanced, the peak cylinder pressures increase from about 90 bar to more than 120 bar, and the location of the peak pressures also moves closer to the TDC. The reasons for these trends can be found in the heat release rate profiles shown in Fig. 12(b). Clearly, the higher T_{in} led to faster pre-ignition reactions and advanced the SOC by more than 10° CA. In addition, the peak heat release rates increased from about 225 J/deg for 75 °C to about 275 J/deg for 105 °C and the location of the peak heat release was also advanced as T_{in} was increased. A direct outcome of faster combustion heat release was shorter combustion durations. The combustion duration decreased by about 10° CA with increasing T_{in}: from more than 40° CA for 75 °C to 30° CA for 105 °C. The overall improvement in the combustion heat release rate, the shorter combustion duration, and the earlier combustion phasing at higher T_{in} are reflected in the fact that a greater fraction of packets reach higher peak temperatures (see Fig. 12(c)). For instance, while no packets attained the peak temperatures in

the 2800–2900 K range for 75 °C, about 7 per cent of the peak packet temperatures fell in this range for 105 °C. On the other hand, as T_{in} was increased from 75 °C to 105 °C, the fraction of packets with peak temperatures lower than 1900 K decreased from 80 per cent to less than 30 per cent. Also, the average peak packet temperatures T_{pPEAK_AVG} increased from 1720 K at 75 °C to 2150 K at 105 °C, which is greater than the $T_{critical\_NO_x}$ value of 2000 K. These trends in the local (packet) temperatures indicate the potential for higher NO_x formation at higher T_{in}.

5.2.2 *Pilot fuel quantity effects*

The effects of Q_{inj} on the predicted cylinder pressure, heat release rate, and peak packet temperature are shown in Fig. 13. As Q_{inj} is increased from 3.3 g/min to 5.4 g/min, ignition occurs earlier, the peak cylinder pressures increase, and the location of the peak pressures occurs closer to the TDC. The heat release rate profiles (see Fig. 13(b)) show that higher Q_{inj} led to a slight advancement of the SOC by about 2° CA, substantially higher peak heat release rates

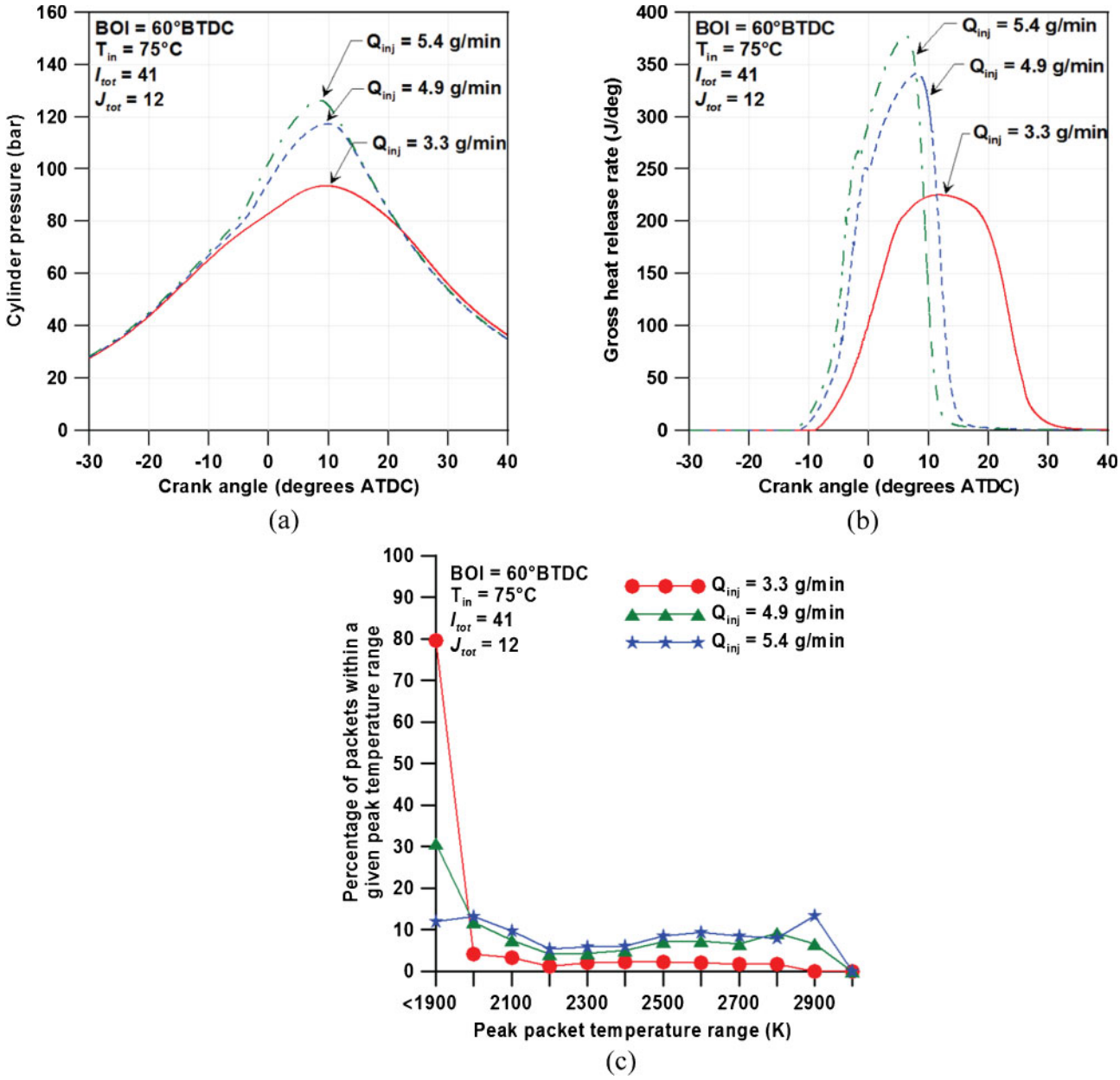

Fig. 13 Effects of the pilot fuel quantity Q_{inj} on (a) the predicted cylinder pressure, (b) the predicted heat release rate, and (c) the predicted peak packet temperature ranges for the 60° before TDC BOI

(from about 225 J/deg for 3.3 g/min to about 375 J/deg for 5.4 g/min), and earlier peak heat release phasing. Higher Q_{inj} resulted in hotter packets that expanded rapidly, increasing the effective flame area and overall combustion rates. Compared with the effects of T_{in}, the SOC advancement was weaker but the peak heat release rates were much higher at higher Q_{inj}. The higher heat release rates resulted in shorter combustion durations (from 40° CA for 3.3 g/min to 25° CA for 5.4 g/min). All these combustion effects at higher Q_{inj} combined to cause more packets to reach higher peak temperatures, as evident from Fig. 13(c). As Q_{inj} was increased from 3.3 g/min to 5.4 g/min, the fraction of low-temperature packets (with peak temperatures lower than 1900 K) decreased from 80 per cent to only 10 per cent while high-temperature packets in the 2800–2900 K range increased from 0 per cent to 14 per cent. With increasing Q_{inj}, T_{pPEAK_AVG} increased from 1720 K at 3.3 g/min to 2270 K at 5.4 g/min. These trends confirm conventional wisdom in dual-fuel combustion, which dictates that a higher Q_{inj} will probably lead to higher NO_x emissions owing to higher local temperatures. Further, when Figs 12 and 13 are compared, the impact of increasing Q_{inj} on the local temperatures (and the NO_x emissions) is clearly more significant than increasing T_{in}.

5.2.3 *Natural-gas equivalence ratio effects*

Figure 14 demonstrates the combustion behaviour for the 60° before TDC BOI at different ϕ_{NG} but fixed Q_{inj} (= 3.3 g/min) and T_{in} (= 75 °C). Since all the other parameters were fixed, increasing ϕ_{NG} from 0.37 to 0.56 led to an overall increase (approximately 40 per cent) in the engine load (IMEP). The cylinder pressure results shown in Fig. 14(a) followed expectations in that the peak pressures increased as the natural-gas equivalence ratio was increased from 0.37 to 0.56. Figures 14(b) and (c) show the heat release profiles and peak packet temperatures respectively at different ϕ_{NG}. First, with increasing ϕ_{NG}, there is a slight (although noticeable) delay in the SOC. Second, the peak heat release rates are significantly higher and the combustion durations are slightly shorter at higher ϕ_{NG}. Third, the initial heat release rates (within the first 10° CA after the SOC) are not affected much by increasing ϕ_{NG} since the initial combustion rates in the packets were probably similar as T_{in} and Q_{inj} were fixed at 75 °C and 3.3 g/min respectively. The influence of ϕ_{NG} is noticeable only later (after TDC) during flame-zone combustion. Finally, the distribution of the peak packet temperatures in most temperature ranges is relatively unaffected by ϕ_{NG} with the exceptions of the temperature ranges below 1900 K and 2700–2800 K. As ϕ_{NG} was increased from 0.37 to 0.56, the fraction of low-peak-temperature (less than 1900 K) packets decreased from 80 per cent to less than 70 per cent while the fraction of high-peak-temperature packets increased from 2 per cent to 10 per cent in the 2700–2800 K range. On the other hand, there was only a small increase in T_{pPEAK_AVG} from 1720 K at $\phi_{NG} = 0.37$ to 1850 K at $\phi_{NG} = 0.56$. While the higher T_{pPEAK_AVG} may lead to slightly higher NO_x emissions at higher ϕ_{NG}, this increase will probably be modest compared with the influences of T_{in} and Q_{inj} on NO_x. This is largely because, as ϕ_{NG} was increased to 0.56, the T_{pPEAK_AVG} value attained was still lower than the critical NO_x formation temperature of 2000 K. Consequently, engine-out NO_x emissions with ALPING combustion remained very low even when the engine load was increased by increasing ϕ_{NG}, a fact that was demonstrated experimentally in previous studies [**18**, **20**].

6 CONCLUSIONS

A multi-zone phenomenological simulation has been developed to simulate partially premixed ALPING LTC. This simulation combined, in a novel way, several modelling aspects of diesel spray combustion and premixed turbulent flame propagation. The cylinder contents were divided into an unburned zone, pilot fuel zones (or 'packets') that account for diesel combustion, a flame zone for natural-gas combustion, and a burned zone. Predictions from the simulation were validated against experimental results and parametric studies were performed, leading to the following significant conclusions.

1. The simulation predicted ALPING LTC satisfactorily over a wide range of pilot injection timings (BOI) from 20° before TDC to 60° before TDC.
2. The onset of ignition (predicted with the Shell autoignition model) and heat release profiles (especially combustion durations) were predicted accurately for the entire BOI range but the peak pressures were slightly overpredicted for the 30°, 40°, and 50° before TDC BOIs. Both the combustion pressure and the heat release profiles were predicted better at early BOIs, which yielded very low NO_x emissions in ALPING combustion experiments.
3. Strong coupling was observed between pilot spray combustion in the packets and premixed turbu-

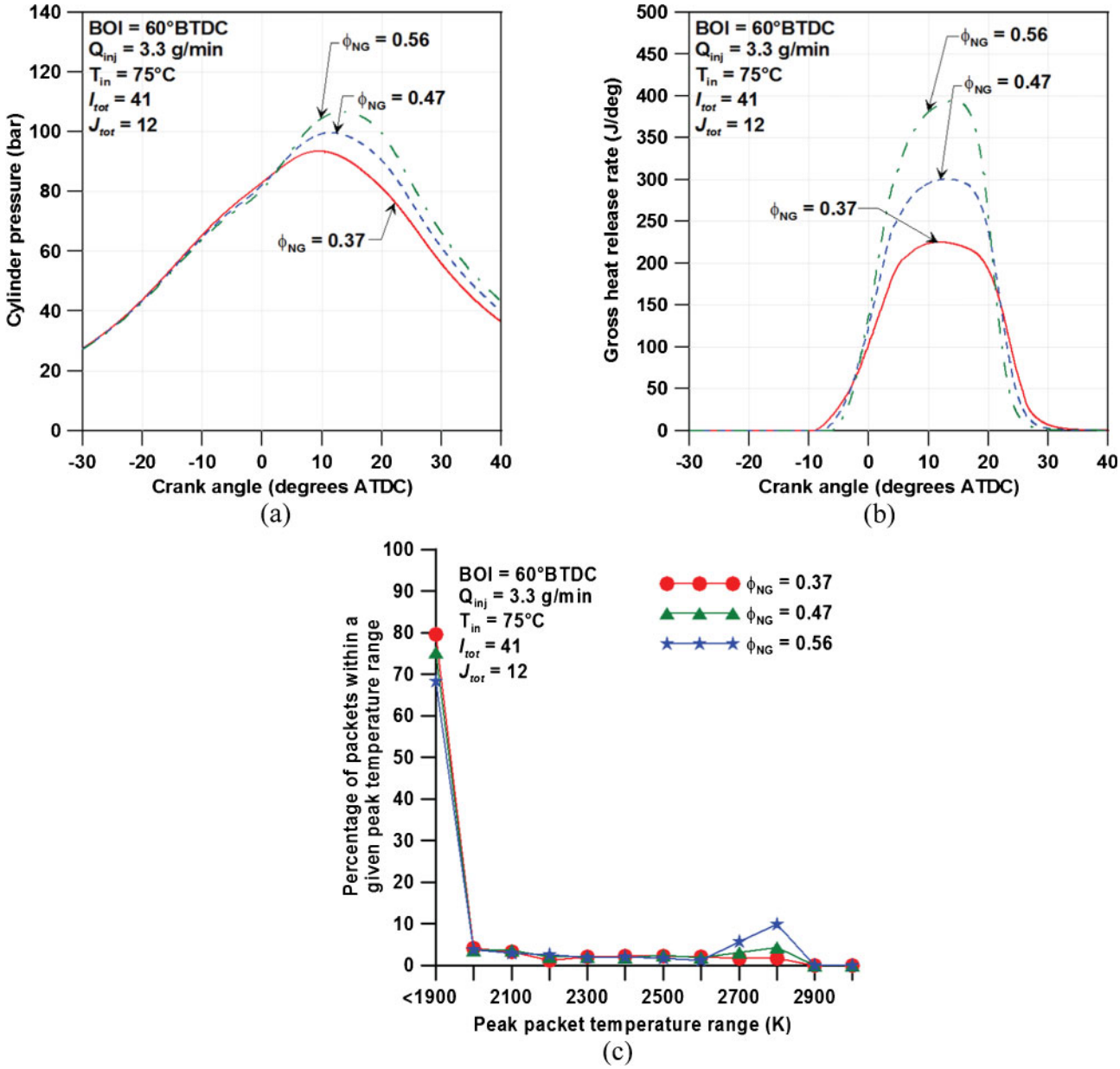

Fig. 14 Effects of the natural-gas equivalence ratio ϕ_{NG} on (a) the predicted cylinder pressure, (b) the predicted heat release rate, and (c) the predicted peak packet temperature ranges for the 60° before TDC BOI

lent combustion in the flame zone because pilot diesel combustion in the packets directly affected the flame area and, consequently, flame-zone combustion. Further, it was shown that the number of ignition centres (packets) had a profound influence on the overall heat release rates and flame-zone combustion.

4. The highest in-cylinder temperatures were obtained in packets, indicating that *pilot diesel spray combustion is probably the dominant source of NO_x emissions in ALPING combustion*. The measured engine-out NO_x emissions were extremely low at the 60° before TDC BOI, probably because of relatively low-temperature packets that persisted longer in the combustion process; further, the average peak packet temperature T_{pPEAK_AVG} was only 1720 K, much lower than the critical NO_x formation temperature $T_{critical\_NO_x}$ of 2000 K. By comparison, at 20° before TDC and 40° before TDC, the peak temperatures of long-residence-time packets were much higher (the T_{pPEAK_AVG} values for 20° before TDC and 40°

before TDC were 2480 K and 2700 K respectively), resulting in substantially higher NO_x emissions.

5. Although approximately 90 per cent of the combustion energy release occurred in the flame zone, the predicted peak flame temperature was only about 1650 K (owing to the very lean flame-zone equivalence ratio of approximately 0.38), indicating the *near-zero potential for NO_x formation in the flame zone*.
6. Increasing the intake charge temperature T_{in} and the pilot fuel quantity Q_{inj} led to faster combustion, higher peak heat release rates, and higher T_{pPEAK_AVG} values at the 60° before TDC BOI, confirming their relative importance vis-à-vis NO_x emissions. However, increasing the natural-gas equivalence ratios ϕ_{NG} at fixed T_{in} and Q_{inj} led to only higher peak heat release rates without affecting the T_{pPEAK_AVG} values significantly. These results are in agreement with experimentally measured trends [**18**, **20**] for NO_x emissions, which were relatively unaffected as ϕ_{NG} was increased (at fixed Q_{inj}) to attain engine loads as high as 12 bar BMEP.

7 FUTURE WORK

In the present work, a phenomenological framework based on pilot diesel spray combustion and premixed turbulent flame propagation was developed to simulate partially premixed ALPING LTC. The simulation integrated pilot spray combustion and premixed turbulent flame combustion through a unique flame area computation methodology. While the present simulation predicted the onset of ignition and heat release trends satisfactorily and revealed several important features of ALPING LTC (including strong coupling between spray combustion and flame propagation), there is room for further improvement. In particular, the spray model can be improved to capture the radial stratification better (instead of using different J_{tot} values at different BOIs), to incorporate a more sophisticated spray penetration model (see, for example, reference [**34**]), and to accommodate possible spray wall impingement at early BOIs. Also, the turbulent flame propagation model and the flame area computation methodology can be refined to eliminate or reduce the dependence of the combustion rate on the number of packets, and to account for possible spatial recombination of enflamed packets, which may reduce the effective flame area during combustion.

ACKNOWLEDGEMENTS

The authors appreciate the partial financial support for this work provided by the Sustainable Energy Research Center at Mississippi State University. In addition, the authors gratefully acknowledge the detailed comments and suggestions for improvement provided by the two anonymous reviewers.

REFERENCES

1 **Zhang, F., Okamoto, K., Morimoto, S.,** and **Shoji, F.** Methods of increasing the BMEP (power output) for natural-gas SI engines. SAE paper 981385, 1998.
2 **Kopecek, H., Wintner, E., Lackner, M., Winter, F.,** and **Hultqvist, A.** Laser-stimulated ignition in a homogeneous charge compression ignition engine. SAE paper 2004-01-0937, 2004.
3 **Bihari, B., Gupta, S. B., Sekar, R. R., Gingrich, J.,** and **Smith, J.** Development of advanced laser ignition system for stationary natural gas reciprocating engines. In Proceedings of the Fall Technical Meeting of the Internal Combustion Engines Division of ASME, Ottawa, Ontario, Canada, 11–14 September 2005, paper ICES2005-1325 (ASME International, New York).
4 **Gebert, K., Beck, N. J., Barkhimer, R. L.,** and **Wong, H.-C.** Strategies to improve combustion and emission characteristics of dual-fuel pilot ignited natural gas engines. SAE paper 971712, 1997.
5 **Workman, J.** and **Beshouri, G. M.** Single cylinder testing of a high pressure electronic fuel injector for low NO_x emission dual fuel engines. Part II: optimization, startability and inflammability testing. *Trans. ASME, J. Engng Gas Turbines Power*, 1990, **112**, 422–430.
6 **Karim, G. A.** Combustion in gas fueled compression: ignition engines of the dual fuel type. *Trans. ASME, J. Engng Gas Turbines Power*, 2003, **125**, 827–836.
7 **Krishnan, S. R., Biruduganti, M., Mo, Y., Bell, S. R.,** and **Midkiff, K. C.** Performance and heat release analysis of a pilot-ignited natural gas engine. *Int. J. Engine Res.*, 2002, **3**(3), 171–184. DOI: 10.1243/14680870260189280.
8 **Galal, M. G., Abdel Aal, M. M.,** and **El Kady, M. A.** A comparative study between diesel and dual-fuel engines: performance and emissions. *Combust. Sci. Technol.*, 2002, **174**, 241–256.
9 **Gebert, K., Beck, N. J., Barkhimer, R. L., Wong, H.-C.,** and **Wells, A. D.** Development of pilot fuel injection system for CNG engine. SAE paper 961100, 1996.
10 **Flynn, P. F., Hunter, G. L., Farrell, L., Durrett, P., Akinyemi, O., Zur Loye, A. O., Westbrook, C. K.,** and **Pitz, W. J.** The inevitability of engine-out NO_x

emissions from spark ignited and diesel engines. *Proc. Combust. Inst.*, 2000, **28**, 1211–1218.

11 **Zhao, F., Asmus, T., Assanis, D., Dec, J. E., Eng, J. A.,** and **Najt, P. M.** *Homogeneous charge compression ignition (HCCI) engines*, 2003 (SAE International, Warrendale, Pennsylvania).

12 **Hasegawa, R.** and **Yanagihara, H.** HCCI combustion in DI diesel engine. SAE paper 2003-01-0745, 2003.

13 **Kimura, S., Aoki, O., Kitahara, Y.,** and **Aiyoshizawa, E.** Ultra-clean combustion technology combining a low-temperature and premixed combustion concept for meeting future emission standards. SAE paper 2001-01-0200, 2001.

14 **Kalghatgi, G., Risberg, P.,** and **Angstrom, H.-E.** Advantages of fuels with high resistance to auto-ignition in late-injection, low-temperature, compression ignition combustion. SAE paper 2006-01-3385, 2006.

15 **Kalghatgi, G.** Auto-ignition quality of practical fuels and implications for fuel requirements of future SI and HCCI engines. SAE paper 2005-01-0239, 2005.

16 **Risberg, P., Kalghatgi, G., Angstrom, H.-E.,** and **Wahlin, F.** Auto-ignition quality of diesel-like fuels in HCCI engines. SAE paper 2005-01-2127, 2005.

17 **Musculus, M. P. B.** Multiple simultaneous optical diagnostic imaging of early-injection low-temperature combustion in a heavy-duty diesel engine. SAE paper 2006-01-0079, 2006.

18 **Krishnan, S. R., Srinivasan, K. K., Singh, S., Bell, S. R., Midkiff, K. C., Gong, W., Fiveland, S. B.,** and **Willi, M.** Strategies for reduced NO_x emissions in pilot ignited natural gas engines. *Trans. ASME, J. Engng Gas Turbines Power*, 2004, **126**, 665–671.

19 **Singh, S., Krishnan, S. R., Srinivasan, K. K., Midkiff, K. C.,** and **Bell, S. R.** Effect of pilot injection timing, pilot quantity, and intake charge conditions on performance and NO_x emissions for an advanced low-pilot-ignited natural gas engine. *Int. J. Engine Res.*, 2004, **5**(4), 329–348. DOI: 10.1243/14680870432322423l.

20 **Srinivasan, K. K., Krishnan, S. R., Singh, S., Midkiff, K. C., Bell, S. R., Gong, W., Fiveland, S. B.,** and **Willi, M.** The advanced low pilot ignited natural gas engine – a combustion analysis. *Trans. ASME, J. Engng Gas Turbines Power*, 2006, **128**, 213–218.

21 **Egolfopoulos, F. N., Holley, A. T.,** and **Law, C. K.** An assessment of the lean flammability of CH_4/air and C_3H_8/air mixtures at engine-like conditions. *Proc. Combust. Inst.*, 2007, **31**, 3015–3022.

22 **Srinivasan, K. K., Krishnan, S. R., Qi, Y., Yang, H.,** and **Midkiff, K. C.** Analysis of diesel pilot-ignited natural gas low-temperature combustion with hot exhaust gas recirculation. *Combust. Sci. Technol.*, 2007, **179**(9), 1737–1776.

23 **Qi, Y., Srinivasan, K. K., Krishnan, S. R., Yang, H.,** and **Midkiff, K. C.** Effect of hot exhaust gas recirculation on the performance and emissions of an advanced injection low pilot-ignited natural gas engine. *Int. J. Engine Res.*, 2007, **8**(3), 289–303. DOI: 10.1243/14680874JER02306.

24 **Jung, D.** and **Assanis, D. N.** Multi-zone DI diesel spray combustion model for cycle simulation studies of engine performance and emissions. SAE paper 2001-01-1246, 2001.

25 **Yoshizaki, T., Nishida, K.,** and **Hiroyasu, H.** Approach to low NO_x and smoke emission engines by using phenomenological simulation. SAE paper 930612, 1993.

26 **Patriotis, E. G.** and **Hountalas, D. T.** Validation of a newly-developed quasi-dimensional combustion model – application on a heavy-duty DI diesel engine. SAE paper 2004-01-0923, 2004.

27 **Hountalas, D. T.** and **Papagiannakis, R. G.** A simulation model for the combustion process of natural gas engines with pilot diesel fuel as an ignition source. SAE paper 2001-01-1245, 2001.

28 **Pirouzpanah, V.** and **Kashani, B. O.** Prediction of major pollutants emission in direct-injection, dual-fuel diesel and natural gas engines. SAE paper 1999-01-0841, 1999.

29 **Liu, Z.** and **Karim, G. A.** A predictive model for the combustion process in dual fuel engines. SAE paper 952435, 1995.

30 **Liu, Z.** and **Karim, G. A.** Simulation of combustion processes in gas-fuelled diesel engines. *Proc. IMechE, Part A: J. Power and Energy*, 1997, **211**(2), 159–169. DOI: 10.1243/0957650971537079.

31 **Khalil, E. B.** and **Karim, G. A.** A kinetic investigation of the role of changes in the composition of natural gas in engine applications. *Trans. ASME, J. Engng Gas Turbines*, 1997, **124**, 404–411.

32 **Kusaka, J., Tsuzuki, K., Daisho, Y.,** and **Saito, T.** A numerical study on combustion and exhaust gas emissions characteristics of a dual-fuel natural gas engine using a multi-dimensional model combined with detailed kinetics. SAE paper 2002-01-1750, 2002.

33 **Dent, J. C.** Basis for the comparison of various experimental methods for studying spray penetration. SAE paper 710571, 1971.

34 **Siebers, D. L.** Scaling liquid-phase fuel penetration in diesel sprays based on mixing-limited vaporization. SAE paper 1999-01-0528, 1999.

35 **Bell, S. R.** *Development of a cycle simulation for a coal-fueled direct-injected, internal combustion engine.* Doctoral dissertation, Texas A&M University, College Station, Texas, USA, 1986.

36 **Kanury, A.** *Introduction to combustion phenomena*, 1975 (Gordon and Breach, New York).

37 **Krishnan, S. R., Srinivasan, K. K.,** and **Midkiff, K. C.** Ignition in pilot-ignited natural gas low temperature combustion: multi-zone modeling and experimental results. In Proceedings of the ASME Internal Combustion Engine Division 2009 Spring Technical Conference, Milwaukee, Wisconsin, USA, 3–6 May 2009, paper ICES 2009-76145 (ASME International, New York).

38 **Krishnan, S. R.** *Experimental investigations and phenomenological simulation of combustion in a*

low pilot-ignited natural gas engine with a focus on advanced injection timings. Doctoral dissertation, University of Alabama, Tuscaloosa, Alabama, USA, 2005.

39 **Halstead, M. P., Kirsch, L. J.,** and **Quinn, C. P.** The autoignition of hydrocarbon fuels at high temperatures and pressures – fitting of a mathematical model. *Combust. Flame*, 1977, **30**, 45–60.

40 **Sazhina, E. M., Sazhin, S. S., Heikal, M. R.,** and **Marooney, C. J.** The Shell autoignition model: applications to gasoline and diesel fuels. *Fuel*, 1999, **78**(4), 389–401.

41 **Westbrook, C. K.** and **Dryer, F. L.** Simplified reaction mechanisms for the oxidation of hydrocarbon fuels in flames. *Combust. Sci. Technol.*, 1981, **27**, 31–43.

42 **Heywood, J. B.** Combustion and its modeling in spark-ignition engines. In Proceedings of the Third International Symposium on *Diagnostics and modeling of combustion in internal combustion engines* (*COMODIA 1994*), Yokohama, Japan, 11–14 July 1994, pp. 1–15 (Engine Systems Division, Japan Society of Mechanical Engineers, Tokyo).

43 **Tabaczynski, R. J., Ferguson, C. R.,** and **Radhakrishnan, K.** A turbulent entrainment model for spark-ignition engine combustion. *Trans. SAE*, 1977, **86**, 2414–2433; also SAE paper 770647, 1977.

44 **Tennekes, H.** Simple model for the small-scale structure of turbulence. *Phys. Fluids*, 1968, **11**(3), 669–671.

45 **Tabaczynski, R. J., Trinker, F. H.,** and **Shannon, B. A. S.** Further refinement and validation of a turbulent flame propagation model for spark-ignition engines. *Combust. Flame*, 1980, **39**(2), 111–121.

46 **Krishnan, S. R.** *Heat release analysis of dual fuel combustion in a direct injection compression-ignition engine*. MS Thesis, University of Alabama, Tuscaloosa, Alabama, USA, 2001.

47 **Turns, S. R.** *An introduction to combustion: concepts and applications,* 2nd edition, 2001 (McGraw-Hill, New York).

48 **Brehob, D. D.** and **Newman, C. E.** Monte Carlo simulation of cycle by cycle variability. SAE paper 922165, 1992.

49 **Shen, H., Hinze, P. C.,** and **Heywood, J. B.** A study of cycle-to-cycle variations in SI engines using a modified quasi-dimensional model. SAE paper 961187, 1996.

50 **Hill, P. G.** Cyclic variations and turbulence structure in spark-ignition engines. *Combust. Flame*, 1988, **72**, 73–89.

51 **Tennekes, H.** and **Lumley, J. L.** *A first course in turbulence*, 1972 (MIT Press, Cambridge, Massachusetts).

52 **Heywood, J. B.** *Internal combustion engine fundamentals*, 1988, p. 143 (McGraw-Hill, New York).

53 **Woschni, G.** A universally applicable equation for the instantaneous heat transfer coefficient in the internal combustion engine. *Trans. SAE*, 1967, **76**, 3065–3083; also SAE paper 670931, 1967.

54 **Hountalas, D. T., Kouremenos, D. A.,** and **Fiveland, S. B.** Some considerations on the estimation of the heat release of DI diesel engines using modeling techniques. SAE paper 2004-01-1405, 2004.

APPENDIX

Notation

ALPING	advanced (injection) low-pilot-ignited natural gas
after TDC	after top dead centre
A_f	flame area
A_{p3}	pre-exponential factor controlling fuel consumption in the propagation cycle of the Shell model
BMEP	brake mean effective pressure
BOI	beginning of (pilot) injection
before TDC	before top dead centre
CA	crank angle
c_b	burned mass fraction exponent in the flame area equation
c_{fdrop}	model constant in the exponential term for flame entrainment
c_v	specific heat at constant volume
C_ϕ	lean packet equivalence ratio exponent
EGR	exhaust gas recirculation
EOC	end of combustion
EOI	end of injection
EPA	(US) Environmental Protection Agency
E_A	activation energy
HC	(unburned) hydrocarbon
HCCI	homogeneous charge compression ignition
h	specific enthalpy
IMEP	indicated mean effective pressure
IVC	intake valve closure
I	packet classification based on their time of entry into the cylinder
J	packet classification accounting for radial stratification in the spray
K	entrainment constant
K_{Af}	flame area proportionality constant
LTC	low-temperature combustion
L	integral length scale
m	mass of different zones
$\dot{m}$	reaction rate or rate of change in the mass
MW	molecular weight
NO_x	oxides of nitrogen

n_{dump}	number of packets that have been dumped
PM	particulate matter
P	instantaneous cylinder pressure
Q	heat release, heat transfer, or pilot quantity (depending on the subscript)
RON	research octane number
R	characteristic gas constant
R_{f}	equivalent flame radius calculated from flame area
SMD	Sauter mean diameter
SOC	start of combustion
S_{L}	laminar burning velocity
TDC	top dead centre
T	temperature
$T_{\text{critical\_NO}_x}$	critical temperature at which NO_x formation becomes significant (about 2000 K)
$T_{\text{pPEAK\_AVG}}$	average peak packet temperature
u	turbulent entrainment velocity
u'	turbulence intensity
V	instantaneous cylinder volume
y_{pb}	packet burned mass fraction
Y	ratio of time elapsed since the BOI to total injection duration
η	Kolmogorov microscale
θ	crank angle
λ	Taylor scale
μ	dynamic viscosity
ν	kinematic viscosity
ρ	density
τ_{b}	characteristic burn time
ϕ	equivalence ratio
ω	crankshaft angular velocity

Subscripts

avg	average (over the entire cylinder)
b	burned zone or burn-related parameter
ch	characteristic
d	diesel
e, ent	entrained
expt	experimental
f	flame zone
i	initial value
in	intake manifold
inj	injected
i	zone index
ij	packet (I, J)
ng, NG	natural gas
p	packets (pilot fuel zones)
sim	simulated
tot	overall, total, or for the entire contents in the cylinder
tot-ent	total entrained
u	unburned zone
wall	cylinder wall